

International Journal of Modern Physics B
Vol. 28, No. 00 (2014) 1430009 (43 pages)
© World Scientific Publishing Company
DOI: 10.1142/S0217979214300096



***Ab initio* calculations of SrTiO₃, BaTiO₃, PbTiO₃, CaTiO₃, SrZrO₃, PbZrO₃ and BaZrO₃ (001), (011) and (111) surfaces as well as *F* centers, polarons, KTN solid solutions and Nb impurities therein**

R. I. Eglitis

*Institute of Solid State Physics, University of Latvia,
8 Kengaraga Str., Riga LV1063, Latvia
rieglitis@gmail.com*

Received 14 February 2014

Accepted 23 February 2014

Published DD MM 2014

In this paper, the review of recent results of calculations of surface relaxations, energetics, and bonding properties for ABO₃ perovskite (001), (011) and (111) surfaces using mostly a hybrid description of exchange and correlation is presented. Both AO and BO₂-terminations of the nonpolar (001) surface and A, BO, and O terminations of the polar (011) surface, as well as B and AO₃-terminations of the polar (111) surface were considered. On the AO-terminated (001) surface, all upper-layer A atoms relax inwards, while all second layer atoms relax outwards. For the BO₂-terminated (001) surface, in most cases, the largest relaxations are on the second-layer metal atoms. For almost all ABO₃ perovskites, the surface rumpling is much larger for the AO-terminated than for the BO₂-terminated (001) surface, but their surface energies are always quite similar. In contrast, different terminations of the (011) ABO₃ surface lead to very different surface energies for the O-terminated, A-terminated, and BO-terminated (011) surface, respectively. A considerable increase in the Ti–O or Zr–O, respectively, chemical bond covalency near the (011) surface as compared both to the bulk and to the (001) surface in ABO₃ perovskites were predicted. According to the results of *ab initio* calculations for Nb doped SrTiO₃, Nb is a shallow donor; six nearest O ions are slightly displaced outwards from the Nb ion. The *F* center in ABO₃ perovskites resembles electron defects in the partially-covalent SiO₂ crystal rather than usual *F* centers in ionic crystals like MgO and alkali halides. The results of calculations for several perovskite KNb_xTa_{1-x}O₃ (KTN) solid solutions, as well as hole and electron polarons in ABO₃ perovskites are analyzed.

Keywords: *Ab initio* calculations; ABO₃ perovskites.

PACS numbers: 68.35.Ct, 68.35.Md, 68.47.Gh

1. Introduction

Oxide perovskites are in demand for a variety of high-tech applications as a result of their diverse physical properties.¹⁻³ Thin films of ABO₃ perovskite ferroelectrics are

R. I. Eglitis

important for many industrial applications including high capacity memory cells, catalysis, optical wave guides, integrated optics applications, substrates for high- T_c cuprate superconductor growth, etc.⁴⁻⁶ For all these applications, the surface structure and the associated surface electronic and chemical properties are of key importance. *Ab initio* calculations of SrTiO₃, BaTiO₃, PbTiO₃, CaTiO₃, SrZrO₃, PbZrO₃ and BaZrO₃ surface characteristics are useful to understand processes in which surfaces play a crucial role, such as the chemistry of surface reactions, interface phenomena, and adsorption. In this study, theoretical calculations dealing with relaxed atomic structures of the SrTiO₃, BaTiO₃, PbTiO₃, CaTiO₃, SrZrO₃, PbZrO₃ and BaZrO₃ (001), (011) and (111) surfaces were reviewed.

Due to intensive development and progressive miniaturization of electronic devices, the surface structure as well as the electronic properties of the ABO₃ perovskite thin films have been extensively studied experimentally in recent years. Among all ABO₃ perovskites, experimentally most intensively have been studied the (001) surface of the technologically very important SrTiO₃ perovskite. For example, Bickel *et al.*⁷ analyzed the (001) surface structure of SrTiO₃ at $T = 120$ K by means of low-energy-electron diffraction (LEED). They got the best theory-experiment fit results for a surface containing domains of two different layer terminations.⁷ Four years later, Hikita *et al.*⁸ experimentally studied the electronic and atomic structure of TiO₂ and SrO terminated SrTiO₃ (100) surface using reflection high energy electron diffraction (RHEED), X-ray photoelectron spectroscopy (XPS) and UPS. According to their results, the oxygen atoms on the outermost SrTiO₃ surface are pulled out for 0.10 Å and 0.16 Å, respectively.⁸ Note, however, that the LEED⁷ and RHEED⁸ experiments contradict each other in the sign of the near-surface interplanar separation between the first and the second surface plane Δd_{12} for SrO-terminated SrTiO₃ (001) surface. Ikeda *et al.*⁹ determined the surface relaxation and rumpling of TiO₂-terminated SrTiO₃ (001) surface by means of medium energy ion scattering (MEIS). Charlton *et al.*¹⁰ used the X-ray diffraction in order to determine the 300 K structure of SrTiO₃ (001) 1×1 with a termination of 78% TiO and 22% of SrO. Their data indicated that a lateral ferroelectric distortion was absent on both terminations.¹⁰ Van der Heide *et al.*¹¹ analyzed the chemical and structural properties of several SrTiO₃ (001) surfaces prior to and following UHV and O₂ annealing using XPS, time-of-flight and recoiling spectrometry (TOF-SARS), and LEED. Their simulations of the TOF-SARS azimuthal scans indicated that the O atoms are located 0.1 Å above the Ti-terminated surface layer.¹¹ Maus-Friedrichs *et al.*¹² experimentally investigated the SrTiO₃ (001) surface with the metastable impact electron spectra (MIES) and ultraviolet photoelectron spectroscopy (UPS) methods, as well as performed complementary *ab initio* calculations.¹²

Enterkin *et al.*¹³ reported a solution to the 3×1 SrTiO₃ (110) surface structure obtained through transmission electron diffraction, and confirmed through density functional theory (DFT) calculations and scanning tunneling microscopy (STM) images and simulations.¹³ In contrast to ABO₃ perovskite (001) surfaces, their (011) surfaces are experimentally considerably less studied. Most of the experimen-

tal work dealing with ABO₃ perovskite (011) surfaces was focused on the SrTiO₃ (011) surface using STM, UPS, XPS techniques, Auger spectroscopies, and LEED experiments.^{14–20}

There exist several experimental studies dealing with SrTiO₃ (111) surfaces. For example, Tanaka and Kawai have obtained clean surfaces of reduced SrTiO₃ (111) crystals and observed them by means of STM combined with reflection high energy diffraction. They have observed two different surface structures. One obtained by annealing at the temperature $\sim 1.180^\circ\text{C}$, is assigned to have a SrO₃ outermost layer. The other, obtained by annealing at the temperature $\sim 1.220^\circ\text{C}$, is assigned to have a Ti outermost layer.²¹ More than 10 years later Chang *et al.*²² also reproducibly obtained an atomically well-defined SrTiO₃ (111) surface by a combined chemical etching and thermal annealing process.

It is not surprising that the high technological importance of SrTiO₃, BaTiO₃, PbTiO₃, CaTiO₃, SrZrO₃, PbZrO₃ and BaZrO₃ perovskites has motivated several *ab initio* and classical shell-model studies of their (001) surfaces.^{23–82} ABO₃ perovskite (011) surfaces, in general, and SrTiO₃ (011) surfaces, in particular, are considerably less well studied than the corresponding (001) surfaces. Due to the very complex polar structure, only very few *ab initio* studies of ABO₃ perovskite (011) surfaces exist. The first *ab initio* study of the electronic and atomic structures of several (1 × 1) terminations of the (011) polar orientation of the SrTiO₃ surface was performed by Bottin *et al.*⁸³ One year later, Heifets *et al.*⁸⁴ performed very comprehensive *ab initio* Hartree–Fock (HF) calculations for four possible terminations (TiO, Sr, and two kinds of O terminations) of the SrTiO₃ (011) surface. Recently, simultaneously, Eglitis⁶⁴ and Heifets *et al.*⁸⁵ performed *ab initio* density-functional calculations of the atomic structure and charge redistribution for several different terminations of the BaZrO₃ (011) surfaces. Regarding other ABO₃ perovskite (011) surfaces, Eglitis and Vanderbilt recently performed first *ab initio* calculations based on hybrid HF and DFT exchange functionals by using Becke’s three-parameter method combined with the nonlocal correlation functionals of Perdew and Wang (B3PW) for the technologically important BaTiO₃ and PbTiO₃ (011) surfaces.⁴⁷ Only two *ab initio* studies exist for the CaTiO₃ (011) surfaces. The *ab initio* study of CaTiO₃ (011) polar surfaces was performed by Zhang *et al.*⁵⁹ and recently also by Eglitis and Vanderbilt.⁵⁷ Finally, first *ab initio* calculations for SrZrO₃ and PbZrO₃ (011) surfaces were performed by Eglitis and Rohlfing.⁶⁸

ABO₃ perovskite polar (111) surfaces, on the theory side, are even less studied than their (011) surfaces. Pojani *et al.*,⁸⁶ relying on the results obtained by a total energy, semi-empirical HF method, discussed polarity effects at the (111) and (110) surfaces of SrTiO₃. For these orientations, they considered some prototypical (1 × 1) configurations, which differ by their surface composition and the coordination number of the surface atoms. They argued that the compensation for these polar orientations is achieved through anomalous filling of surface states, which, in principle, should be detectable by surface spectroscopies. Only three theoretical

R. I. Eglitis

ab initio studies up to now exist dealing with CaTiO_3 (111) polar surfaces. Liu *et al.*⁸⁷ constructed the stoichiometric and nonstoichiometric terminations for the CaTiO_3 (111) surface. The cleavage and surface energies, surface grand potential, and surface electronic structure have been calculated for the two main classes of terminations using an *ab initio* plane wave ultrasoft pseudopotential method based on the local density approximation (LDA). Some preliminary results of *ab initio* B3LYP calculations for CaTiO_3 (111) surfaces are reported in Ref. 88. One year later, Eglitis and Rohlfiing^{89,90} performed *ab initio* calculations dealing with CaTiO_3 and SrTiO_3 polar (111) surface relaxations, rumplings, energetics, optical bandgaps, and charge distributions using the *ab initio* code CRYSTAL and a hybrid description of exchange and correlation. Finally, Eglitis performed the first *ab initio* calculations for polar BaTiO_3 , BaZrO_3 and SrZrO_3 (111) surfaces.^{91–93}

ABO_3 perovskite-type oxide crystals have numerous technological applications, and in particular, KNbO_3 , KTaO_3 and their solid solutions $\text{KTa}_{1-x}\text{Nb}_x\text{O}_3$ (KTN) are used in electro-optics, holography, and second-harmonic generation applications.⁹⁴ As the temperature decreases, KNbO_3 goes through three ferroelectric phase transitions, whereas KTaO_3 is only an *incipient* ferroelectric which becomes ferroelectric already at very low Nb impurity concentrations, $x \geq 0.01$. This raises a question about the nature of the phase transition in KTN.⁹⁵ XPS has shown⁹⁶ that Ta ions are replaced by the Nb ions. Additionally XAFS measurements⁹⁵ have demonstrated that the Nb sits in off-center positions. Its [111] displacement is 0.145 Å at 70 K, and changes less than 20% as the temperature increases to the room temperature.

Nb-doped SrTiO_3 is also important for several high tech applications including anodes and cathodes of solid oxide fuel cells^{97,98} and nonvolatile resistive switching memories.⁹⁹ Donor-doped SrTiO_3 ceramics have found applications also in sensors, varistors, grain boundary layer capacitors and catalysts. For these reasons, a detailed understanding of the bulk and surface structure and electronic properties of Nb doped SrTiO_3 is of primary importance. Considering high technological importance of Nb doped SrTiO_3 , it is not surprising that during the last years it has been the subject of many experimental studies,^{100–102} but better theoretical understanding is still necessary. The existing *ab initio* calculations were performed using DFT method combined with the plane wave basis set (BS) (CASTEP computer code),¹⁰³ full-potential linearized augmented plane waves (FLAPW)¹⁰⁴ and linear muffin–tin orbital approach (LMTO-ASA).¹⁰⁵ The common disadvantage of the DFT method is considerable underestimate of the bandgap of solids, typically 1.5–2.0 eV for SrTiO_3 instead of the experimental value of 3.3 eV. Due to this fact in most DFT calculations, energy levels of donors fall erroneously into the conduction band. The second DFT problem is lack of analysis of effective atomic charges and charge redistribution caused by defects. Lastly, in most of these calculations rather small supercells were used, which do not eliminate artificial interaction of periodically distributed Nb ions. Finally, Eglitis and Kotomin¹⁰⁶ performed the HF calculations, which typically overestimates the bandgap.

Ab initio calculations of ABO₃ perovskite surfaces and defects

Along with the impurities, most of the real crystals are nonstoichiometric and thus contain large concentration of intrinsic defects vacancies. Oxygen vacancies are known to give rise to F^+ and F centers (vacancy with trapped one or two electrons, respectively).^{107–110} Properties of F -type centers, as well as hole and electron polarons, in ionic oxides are well studied. In this paper, the latest results dealing with large-scale computer modeling of basic point defects — F centers, hole and electron polarons in ABO₃ perovskites were discussed.

2. Preliminaries

2.1. Computational method for surface calculations

First-principles calculations in the framework of DFT using the CRYSTAL computer code¹¹¹ have been carried out. Unlike the plane-wave codes employed in many previous studies,^{112,113} CRYSTAL uses localized Gaussian-type BSs. In calculations by Eglitis and co-workers, the BSs were developed for SrTiO₃, BaTiO₃ and PbTiO₃ in Ref. 114. In this paper, for most of the calculations, for O atoms, this new BS which differs from previous calculations^{29,30} by inclusion of polarizable d -orbitals on O ions were used. The CRYSTAL BS are believed to be largely transferable, so that, once determined for some chemical constituent, they may be successfully applied in the calculations for a variety of chemical substances, for example SrF₂, BaF₂ and CaF₂,^{115–124} where the latter participates. Most of the calculations in this review were performed using the hybrid exchange-correlation B3PW functional involving a mixture of nonlocal Fock exact exchange, local-density approximation (LDA) exchange, and Becke's gradient corrected exchange functional,¹²⁵ combined with the nonlocal gradient corrected correlation potential of Perdew and Wang.^{126–128} The hybrid B3PW functional for most of ABO₃ perovskite surface studies were selected because it yields excellent results for the SrTiO₃, BaTiO₃, and PbTiO₃ bulk lattice constant and bulk modulus.^{29,114}

The reciprocal-space integration was performed by sampling the Brillouin zone, in most cases, with an $8 \times 8 \times 8$ Pack–Monkhorst mesh,¹²⁹ which provides a balanced summation in direct and reciprocal spaces. To achieve high accuracy, large enough tolerances of 7, 8, 7, 7 and 14 were chosen for the dimensionless Coulomb overlap, Coulomb penetration, exchange overlap, first exchange pseudo-overlap, and second exchange pseudo-overlap parameters, respectively.¹¹¹ An advantage of the CRYSTAL code is that it treats isolated two-dimensional slabs, without any artificial periodicity in the z direction perpendicular to the surface, as commonly employed in most previous surface band-structure calculations (e.g., Ref. 41).

The elastic constants are calculated in the standard way.^{111,130} The bulk modulus could be calculated in two ways, first as

$$B = \frac{2}{9V_0} \frac{\partial^2 E_{\text{un.cell}}}{\partial V^2}, \quad (1)$$

R. I. Eglitis

or using the elastic constants¹¹¹:

$$B = (C_{11} + 2C_{12})/3. \quad (2)$$

The results for both type of bulk modulus were presented in Ref. 114.

2.2. ABO_3 perovskite surface geometries

The $SrTiO_3$ (001) surfaces were modeled using symmetric (with respect to the mirror plane) slabs consisting of seven alternating TiO_2 and SrO layers, respectively. (Henceforth, $SrTiO_3$ will be used for presentation purposes, but everything that is said will apply equally to the $BaTiO_3$, $PbTiO_3$, $CaTiO_3$, $SrZrO_3$, $PbZrO_3$ and $BaZrO_3$ cases). One of these slabs was terminated by SrO planes for the $SrTiO_3$ crystal and consisted of a supercell containing 17 atoms. The second slab was terminated by TiO_2 planes and consisted of a supercell containing 18 atoms. These slabs are nonstoichiometric, with unit cell formulas $Sr_4Ti_3O_{10}$ and $Sr_3Ti_4O_{11}$ for the $SrTiO_3$ perovskite. These two (SrO and TiO_2) terminations are the only two possible flat and dense (001) surfaces for the $SrTiO_3$ perovskite lattice structure. The sequence of layers with definition of surface rumpling s and the near-surface interplanar separations Δd_{12} and Δd_{23} at the TiO_2 -terminated (001) surface of $SrTiO_3$ is illustrated in Fig. 1.

Unlike the (001) cleavage of $SrTiO_3$, which naturally gives rise to nonpolar SrO and TiO_2 terminations, a naive cleavage of $SrTiO_3$ to create (011) surfaces leads to the formation of polar surfaces. For example, the stacking of the $SrTiO_3$ crystal along the [011] direction consists of alternating planes of O_2 and $SrTiO$ units having nominal charges of $-4e$ and $+4e$, respectively, assuming O^{2-} , Ti^{4+} , and Sr^{2+} constituents. Thus, a simple cleavage leads to O_2 -terminated and $SrTiO$ -terminated (011) surfaces that are *polar* and have nominal surface charges of $-2e$ and $+2e$

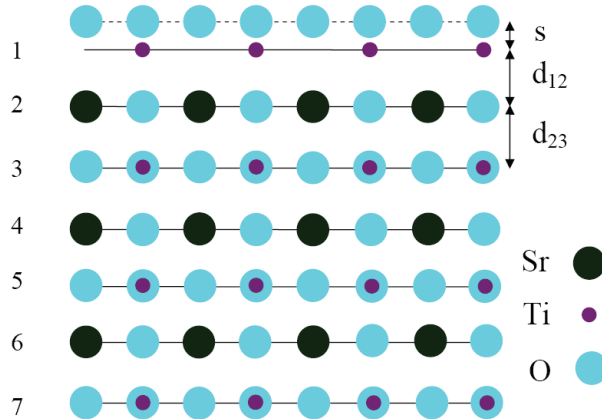


Fig. 1. TiO_2 -terminated $SrTiO_3$ (001) surface with definitions of surface rumpling s and the near-surface interplanar separations Δd_{12} and Δd_{23} .

Ab initio calculations of ABO_3 perovskite surfaces and defects

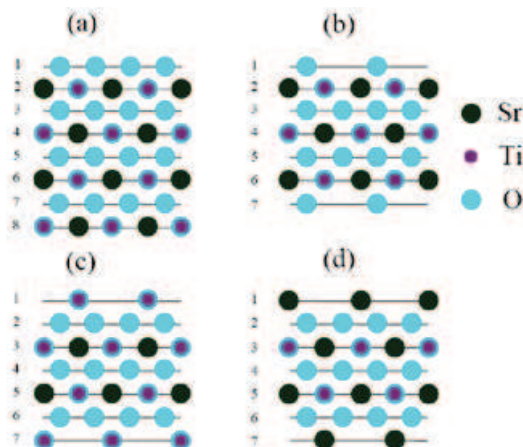


Fig. 2. Side views of slab geometries used to study SrTiO₃ (011) surfaces. (a) Stoichiometric eight-layer slab with O₂-terminated and SrTiO-terminated surfaces at top and bottom, respectively. (b) Seven-layer slab with O-terminated surfaces. (c) Seven-layer slab with TiO-terminated surfaces. (d) Seven-layer slab with Sr-terminated surfaces.

per surface cell, respectively. These are shown as the top and bottom surfaces in Fig. 2(a), respectively. If uncompensated, the surface charge would lead to an infinite electrostatic cleavage energy. In reality, the polar surfaces would probably become metallic in order to remain neutral, but in view of the large electronic gaps in the perovskites, such metallic surfaces would presumably be unfavorable. Thus, we may expect rather generally that such polar crystal terminations are relatively unstable in this class of materials.⁴

On the other hand, if the cleavage occurs in such a way as to leave a half layer of O₂ units on each surface, we obtain the nonpolar surface structure shown in Fig. 2(b). Every other surface O atom has been removed, and the remaining O atoms occupy the same sites as in the bulk structure. We shall refer to this as the “O-terminated” (011) surface, in distinction to the “O₂-terminated” polar surface already discussed in Fig. 2(a). The nonpolar nature of the O-terminated surface can be confirmed by noting that the 7-layer 15-atom Sr₃Ti₃O₉ slab shown in Fig. 2(b), which has two O-terminated surfaces, is neutral. It is also possible to make nonpolar TiO-terminated and Sr-terminated surfaces, as shown in Figs. 2(c) and 2(d), respectively. This is accomplished by splitting a SrTiO layer during cleavage, instead of splitting an O₂ layer. For the TiO- and Sr-terminated surfaces, we use seven-layer slabs having composition Sr₂Ti₄O₁₀ (16 atoms) and Sr₄Ti₂O₈ (14 atoms) as shown in Figs. 2(c) and 2(d), respectively. These are again neutral, showing that the surfaces are nonpolar (even though they no longer have precisely the bulk SrTiO₃ stoichiometry).

As a next step, the ABO₃ perovskite (111) surfaces will be discussed. For example, in Ref. 92, the BaZrO₃ (111) surfaces have been modeled with two-dimensional

R. I. Eglitis

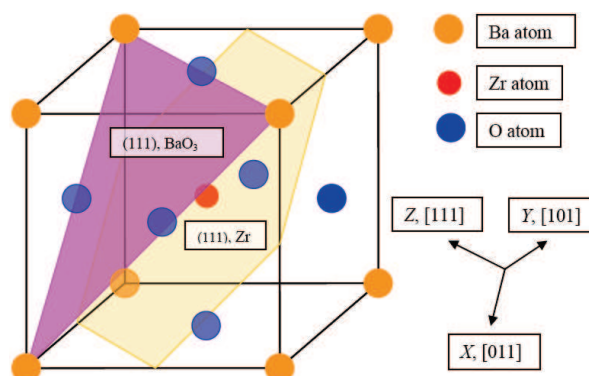


Fig. 3. Sketch of the cubic BaZrO_3 perovskite structure showing two possible (111) surface terminations: BaO_3 and Zr.

(2D) slabs, consisting of nine planes perpendicular to the [111] crystal direction. To simulate BaZrO_3 (111) surfaces, symmetrical slabs consisting of nine alternating Zr and BaO_3 layers were used (see Fig. 3). One of these slabs is terminated by Zr planes and consists of a supercell containing 21 atoms (Zr– BaO_3 –Zr– BaO_3 –Zr– BaO_3 –Zr– BaO_3 –Zr) [see Fig. 4(a)]. The second slab is terminated by BaO_3 planes and consists of a supercell containing 24 atoms (BaO_3 –Zr– BaO_3 –Zr– BaO_3 –Zr– BaO_3 –Zr– BaO_3) [see Fig. 4(b)]. These slabs are nonstoichiometric, with unit cell formulas $\text{Ba}_4\text{Zr}_5\text{O}_{12}$ and $\text{Ba}_5\text{Zr}_4\text{O}_{15}$, respectively (see Fig. 3). As it is well known from previous studies dealing with polar CaTiO_3 and SrTiO_3 (111) surfaces,^{86–89,131} a strong electron redistribution takes place for such terminations in order to cancel the polarity, but the Zr or BaO_3 -terminated BaZrO_3 (111) surface keeps its insulating character, and

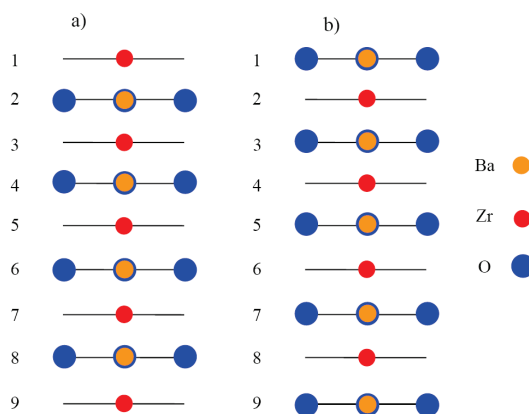


Fig. 4. Sketch of the side views of slab geometries used to study BaZrO_3 (111) surfaces. (a) Nonstoichiometric nine-layer slab with Zr-terminated surfaces. (b) Nonstoichiometric nine-layer slab with BaO_3 -terminated surfaces.

Ab initio calculations of ABO₃ perovskite surfaces and defects

such calculations are feasible. Of course, it is not possible to perform calculations for asymmetric slabs with different terminations, for example, Zr–BaO₃–Zr–BaO₃–Zr–BaO₃–Zr–BaO₃, since this would lead to a large dipole moment for an asymmetric slab.

The second well established approach for ABO₃ perovskite polar (111) surface calculations, which was not used by Eglitis *et al.*⁸⁷ for SrTiO₃, BaTiO₃, CaTiO₃, SrZrO₃ and BaZrO₃ (111) surfaces, is artificial modification of surface structure by removing O atoms from the BaO₃-terminated BaZrO₃ (111) surface and adding O atoms onto the Zr-terminated surface, respectively. Such surface structure changes, (BaO₂–Zr–BaO₃–Zr–BaO₃–Zr–BaO₃–Zr–BaO₂) or (ZrO–BaO₃–Zr–BaO₃–Zr–BaO₃–Zr–BaO₃–ZrO) can, in principle, provide the polarity compensation and calculations for such artificially neutral BaZrO₃ (111) surfaces may also be feasible.

2.3. ABO₃ perovskite surface energies

In order to calculate ABO₃ perovskite, for example, the SrZrO₃ (001) surface energy, I started with the cleavage energy for unrelaxed SrO- and ZrO₂-terminated (001) surfaces. Surfaces with both terminations simultaneously arise under (001) cleavage of the crystal, and I adopt the convention that the cleavage energy is equally distributed between the created surfaces. In my calculations, the nine-layer SrO-terminated (001) slab with 22 atoms and the ZrO₂-terminated one with 23 atoms represent, together, nine bulk unit cells (45 atoms) so that

$$E_{\text{surf}}^{\text{unr}}(\Omega) = \frac{1}{4}[E_{\text{slab}}^{\text{unr}}(\text{SrO}) + E_{\text{slab}}^{\text{unr}}(\text{ZrO}_2) - 9E_{\text{bulk}}], \quad (3)$$

where Ω denotes SrO or ZrO₂, $E_{\text{slab}}^{\text{unr}}(\Omega)$ are the unrelaxed energies of the SrO- or ZrO₂-terminated (001) slabs, E_{bulk} is the energy per bulk unit cell, and the factor of 1/4 comes from the fact that I create four surfaces upon the crystal cleavage procedure. Next, I can calculate the relaxation energies for each of SrO and ZrO₂ terminations, when both sides of the slabs relax, according to

$$E_{\text{rel}}(\Omega) = \frac{1}{2}[E_{\text{slab}}^{\text{rel}}(\Omega) - E_{\text{slab}}^{\text{unr}}(\Omega)], \quad (4)$$

where $E_{\text{slab}}^{\text{rel}}(\Omega)$ is the slab energy after relaxation (and again $\Omega = \text{SrO}$ or ZrO_2). The surface energy is then defined as a sum of the cleavage and relaxation energies,

$$E_{\text{surf}}(\Omega) = E_{\text{surf}}^{\text{unr}}(\Omega) + E_{\text{rel}}(\Omega). \quad (5)$$

In order to calculate the SrZrO₃ (011) surface energies for the ZrO- and Sr-terminated surfaces, I consider the cleavage of eight bulk unit cells (40 atoms) to result in the ZrO- and Sr-terminated slabs, containing 21 and 19 atoms, respectively. I again divide the cleavage energy equally between these two surfaces and obtain

$$E_{\text{surf}}^{\text{unr}}(\Omega) = \frac{1}{4}[E_{\text{slab}}^{\text{unr}}(\text{Sr}) + E_{\text{slab}}^{\text{unr}}(\text{ZrO}) - 8E_{\text{bulk}}], \quad (6)$$

R. I. Eglitis

where Ω denotes Sr or ZrO, $E_{\text{slab}}^{\text{unr}}(\Omega)$ is the energy of the unrelaxed Sr- or ZrO-terminated (011) slab, and E_{bulk} is the SrZrO₃ energy per bulk unit cell.

Finally, when I cleave the SrZrO₃ crystal in another way, I obtain two identical O-terminated (011) surface slabs containing 20 atoms each. This allows for me to simplify the calculations since the unit cell of the nine-plane O-terminated (011) slab contains four bulk unit cells. Therefore, the relevant surface energy is

$$E_{\text{surf}}(\text{O}) = \frac{1}{2}[E_{\text{slab}}^{\text{rel}}(\text{O}) - 4E_{\text{bulk}}], \quad (7)$$

where $E_{\text{surf}}(\text{O})$ and $E_{\text{slab}}^{\text{rel}}(\text{O})$ are the surface energy and the relaxed slab total energy for the O-terminated (011) surface. The ABO₃ perovskite polar (111) surface energy calculations, using as an example the BaZrO₃ crystal, were discussed in Ref. 92.

2.4. Intermediate neglect of different overlap (INDO) method

For defect calculations in ABO₃ perovskites the INDO method was used. The calculation scheme of the Hartree–Fock–Roothaan method in the INDO approximation is discussed in detail in Refs. 132–134. Basically, the procedure reduces to diagonalizing the matrix of the Fock operator to get the one-electron energies, and the linear combination of matrix elements with appropriate weights, depending on the occupation of corresponding one-electron states, provides the total energy. The fixed BS, for example for KNbO₃, is minimal in the sense that each of the atom-centered functions related to the valence-band states (four in total per oxygen atom, nine per transition-metal atom) is encountered only once. The construction of the on-site and off-diagonal parts of the Fock matrix is determined in terms of several empirical parameters, labeled by the atom type A and the index of the atomic orbital (AO) μ (see Refs. 132–134). The interaction of an electron in the μ th valence AO on atom A with its own core

$$U_{\mu\mu}^A = -E_{\text{neg}}^A(\mu) - \sum_{\nu \in A} \left(P_{\nu\nu}^{(0)A} \gamma_{\mu\nu} - \frac{1}{2} P_{\nu\nu}^{(0)A} K_{\mu\nu} \right) \quad (8)$$

contains, apart from the ζ_{μ} value, which specifies the Slater exponent for a one-exponential basis function and hence Coulomb and exchange integrals $\gamma_{\mu\nu}$ and $K_{\mu\nu}$, the initial guesses for the diagonal elements of the density matrix $P_{\mu\mu}^{(0)A}$ and for the energy of μ th AO $E_{\text{neg}}^A(\mu)$, i.e., the ion's electronegativity. The interaction of the μ th AO with the core of another atom B is approximated as

$$V_{\mu}^B = Z_B [1/R_{AB} + [\langle \mu\mu | \nu\nu \rangle - 1/R_{AB}] \exp(-\alpha_{AB} R_{AB})], \quad (9)$$

where R_{AB} is the distance between atoms A and B , Z_B is the core charge of atom B , and parameter α_{AB} describes the nonpoint character of this interaction.

Finally, the resonance-integral parameter $\beta_{\mu\nu}$ enters the off-diagonal Fock matrix elements for the spin component u

$$F_{\mu\nu}^u = \beta_{\mu\nu} S_{\mu\nu} - P_{\mu\nu}^u \langle \mu\mu | \nu\nu \rangle, \quad (10)$$

Ab initio calculations of ABO₃ perovskite surfaces and defects

where the μ th and ν th AO are centered at different atoms, $S_{\mu\nu}$ is the overlap matrix between them, and $\langle\mu\mu|\nu\nu\rangle$ are two-electron integrals. Parameters ζ_μ , $\beta_{\mu\nu}$, α_{AB} and $E_{\text{neg}}^A(\mu)$ are usually fixed throughout the iterations, whereas $P_{\nu\nu}^{(0)A}$ may be corrected as the self-consistency is being achieved.

3. Main Results

3.1. ABO₃ perovskite (001) surface structure

In order to check how sensitive ABO₃ perovskite surface relaxation properties are to details of the *ab initio* methods used in calculations, i.e., exchange–correlation functionals, pseudopotentials, and localized/plane wave BS, in Refs. 29 and 114 were performed a detailed comparative study based on a number of different techniques. Several methods were employed: HF with different DFT-type *a posteriori* electron correlation corrections to the total energy¹³⁵ such as generalized gradient approximation (HFGGA), Perdew-91 (HFPer91), Lee, Yang, Parr (HFLYP) and full-scale DFT calculations based on the Kohn–Sham equation with a number of exchange–correlation functionals, including LDA, generalized gradient approximations (GGA) by Perdew and Wang (PW), Perdew, Burke, and Ernzerhof (PBE), as well as Becke exchange functional with Lee–Yang–Parr correlation functional (BLYP). Also a comparison with hybrid HF–DFT exchange functionals were included, in which HF exchange was mixed with DFT exchange functionals using Becke’s three parameter method, combined with the nonlocal correlation functionals by Perdew and Wang (B3PW), as those by Lee, Yang, and Parr (B3LYP). For all calculations, the CRYSTAL computer code was used (see Ref. 111, and references therein for all mentioned techniques), in which both (HF/DFT) types of calculations are implemented on equal grounds.

Before starting the ABO₃ perovskite (001), (011) and (111) surface structure calculations, these methods were tested on the bulk properties, the lattice constant a_0 , the bulk modulus B and the elastic constants C (see Table 1). It is clear from Table 1 that the LDA calculations, as usually, underestimate the lattice constant for six from seven calculated ABO₃ perovskites. The only exception is SrZrO₃, where the LDA slightly overestimate the lattice constant. The LDA is known to generally underestimate lattice parameters of solids, typically by 1%–3%. This is a serious problem for the study of ferroelectric perovskites using the LDA. As we can see from Table 1, in most cases, pure HF and GGA overestimate the ABO₃ perovskite lattice constant. The different GGA schemes give quite good results only for PbTiO₃ crystal. The PbTiO₃ lattice constants computed using PWGGA and PBE functionals are close to the experimental values, whereas in other cases the DFT–GGA gives mostly overestimated values. The best agreement with experimental lattice constant, on the average, was obtained for the hybrid DFT B3PW method.

Table 1 also lists the computed bulk modulus and the static elastic constants obtained by means of all methods. The presented results for both ways of bulk

R. I. Eglitis

Table 1. The optimized lattice constant a_0 (Å), bulk modulus B (GPa) and elastic constants C_{ij} (in 10^{11} dyne/cm²) for seven ABO₃ perovskites as calculated using DFT and HF methods.

Crystal	Property	LDA	PWGGA	PBE	BLYP	B3PW	B3LYP	HF	Exp
SrTiO ₃	a_0	3.86 ^a	3.95 ^a	3.94 ^a	3.98 ^a	3.90 ^a	3.94 ^a	3.92 ^a	3.89 ^b
	C_{11}	42.10 ^a	31.29 ^a	31.93 ^a	29.07 ^a	31.60 ^a	32.83 ^a	41.68 ^a	31.72 ^c
	C_{12}	12.21 ^a	9.80 ^a	9.75 ^a	9.39 ^a	9.27 ^a	10.57 ^a	7.11 ^a	10.25 ^c
	C_{44}	13.32 ^a	11.34 ^a	11.30 ^a	11.09 ^a	12.01 ^a	12.46 ^a	10.50 ^a	12.35 ^c
	B	222 ^a	170 ^a	171 ^a	159 ^a	167 ^a	180 ^a	186 ^a	174 ^c
BaTiO ₃	a_0	3.96 ^a	4.03 ^a	4.03 ^a	4.08 ^a	4.01 ^a	4.04 ^a	4.01 ^a	4.00 ^b
	C_{11}	35.81 ^a	30.11 ^a	31.04 ^a	28.22 ^a	31.12 ^a	29.75 ^a	30.07 ^a	20.60 ^b
	C_{12}	11.52 ^a	10.35 ^a	10.72 ^a	10.78 ^a	11.87 ^a	11.57 ^a	13.46 ^a	14.00 ^b
	C_{44}	14.98 ^a	13.22 ^a	13.98 ^a	12.24 ^a	14.85 ^a	14.54 ^a	17.34 ^a	12.60 ^b
	B	196 ^a	169 ^a	175 ^a	166 ^a	183 ^a	176 ^a	190 ^a	162 ^b
PbTiO ₃	a_0	3.93 ^a	3.96 ^a	3.96 ^a	4.02 ^a	3.93 ^a	3.96 ^a	3.94 ^a	3.97 ^e
	C_{11}	45.03 ^a	32.47 ^a	4.25 ^q	23.03 ^a	43.04 ^a	34.42 ^a	39.83 ^a	22.90 ^f
	C_{12}	26.14 ^a	15.81 ^a	15.52 ^a	9.93 ^a	24.95 ^a	18.08 ^a	16.90 ^a	10.10 ^f
	C_{44}	11.28 ^a	10.69 ^a	10.96 ^a	8.25 ^a	10.93 ^a	10.35 ^a	17.20 ^a	10.00 ^f
	B	324 ^a	213 ^a	217 ^a	143 ^a	310 ^a	235 ^a	16.90 ^a	144 ^f
CaTiO ₃	a_0	3.825 ^j		3.87 ⁱ		3.85 ^g	3.85 ^k	3.90 ^h	
	B	321 ^a	246 ^a	252 ^a	140 ^a	279 ^a	242 ^a	299 ^a	
BaZrO ₃	a_0	4.16 ^p	4.25 ^q	4.24 ^o		4.23 ^l	4.23 ⁿ	4.19 ^m	
PbZrO ₃	a_0	4.12 ^u				4.18 ^r	4.22 ^t	4.16 ^s	
SrZrO ₃	a_0	4.16 ^v		4.19 ^w		4.17 ^x	4.20 ^t	4.11 ^v	

^aReference 114.

^bReference 136.

^cReference 137.

^dReference 138.

^eReference 139.

^fReference 140.

^gReference 57.

^hReference 141.

ⁱReference 59.

^jReference 142.

^kReference 88.

^lReference 64.

^mReference 143.

ⁿReference 92.

^oReference 145.

^pReference 144.

^qReference 145.

^rReference 146.

^sReference 147.

^tReference 68.

^uReference 148.

^vReference 149.

^wReference 150.

^xReference 67.

^yReference 151.

modulus evaluation differ usually no more than 10–15%. Calculations¹¹⁴ confirm the tendency, well known in the literature, that the HF calculations overestimate the elastic constants. The overestimated elastic constants have also been obtained for SrTiO₃, BaTiO₃ and PbTiO₃ perovskites, when the DFT–LDA scheme was used. In the case of cubic SrTiO₃, which is experimentally well investigated, almost perfect coincidence with the experimental data for both the bulk modulus and elastic constants were obtained using B3PW and B3LYP hybrid schemes. The disagreement of elastic constants is less than 5%, and the bulk modulus practically coincide with the experimental magnitudes.

To characterize the chemical bonding and covalency effects, a standard Mulliken population analysis for the effective static atomic charges Q and other local properties of the electronic structure as described in Refs. 152 and 153 were used. The results from Refs. 25, 47, 57, 64 and 68 for SrTiO₃, BaTiO₃, PbTiO₃, CaTiO₃, BaZrO₃, SrZrO₃ and PbZrO₃ perovskites are presented in Table 2. For example, calculated effective charges for bulk PbTiO₃ are +1.354 e for the Pb atom, +2.341 e for the Ti atom, and –1.232 e for the O atom.⁴⁷ The bond population describing the chemical bonding between Ti and O atoms is +98 me , typical also for another ABO₃ perovskites. Calculated effective charges for BaTiO₃ bulk are +1.797 e for the Ba atom, +2.367 e for the Ti atom, and –1.388 e for the O atom,⁴⁷ indicating a

Ab initio calculations of ABO₃ perovskite surfaces and defects

Table 2. Effective charges Q and bond populations P of atoms in SrTiO₃, BaTiO₃, PbTiO₃, CaTiO₃, BaZrO₃, SrZrO₃ and PbZrO₃ bulk calculated by means of the hybrid B3PW or B3LYP method.

SrTiO ₃		BaTiO ₃		PbTiO ₃		CaTiO ₃		BaZrO ₃		SrZrO ₃		PbZrO ₃		
Prop.	Ion	B3PW	Ion	B3PW	Ion	B3PW	Ion	B3PW	Ion	B3PW	Ion	B3LYP	Ion	B3LYP
Q	Sr	1.871 ^a	Ba	1.797 ^b	Pb	1.354 ^b	Ca	1.782 ^c	Ba	1.815 ^d	Sr	1.880 ^e	Pb	1.368 ^e
P	O	-10	O	16	O	16	O	6	O	-12	O	2	O	30
Q	O	-1.407	O	-1.388	O	-1.232	O	-1.371	O	-1.316	O	-1.351	O	-1.160
P	O	88	O	98	O	98	O	84	O	108	O	92	O	106
Q	Ti	2.351	Ti	2.367	Ti	2.341	Ti	2.330	Zr	2.134	Zr	2.174	Zr	2.111

^aReference 25. ^bReference 47. ^cReference 57. ^dReference 64. ^eReference 68.

R. I. Eglitis

Table 3. The calculated optical bandgaps (in electron volts) for the SrTiO₃, BaTiO₃, PbTiO₃, BaZrO₃ and SrZrO₃ bulk using different exchange–correlation functionals.

Crystal	Gap	LDA	PWGGA	PBE	BLYP	B3PW	B3LYP	HF	Exp.
SrTiO ₃	Γ–Γ	2.36 ^a	2.31 ^a	2.35 ^a	2.27 ^a	3.96 ^a	3.89 ^a	12.33 ^a	3.75 ^b
BaTiO ₃	Γ–Γ	1.98 ^a	1.97 ^a	1.99 ^a	1.91 ^a	3.55 ^a	3.49 ^a	11.73 ^a	3.2 ^c
PbTiO ₃	Γ–Γ	2.65 ^a	2.61 ^a	2.65 ^a	2.48 ^a	4.32 ^a	4.15 ^a	12.74 ^a	3.4 ^d
BaZrO ₃	Γ–Γ	3.2 ^e		3.10 ^f			4.79 ^g		5.0 ^h
SrZrO ₃	Γ–Γ		3.53 ⁱ	3.52 ⁱ			5.31 ⁱ		5.6 ^j

^aReference 114. ^bReference 155. ^cReference 156. ^dReference 157. ^eReference 158.

^fReference 77. ^gReference 92. ^hReference 159. ⁱReference 68. ^jReference 160.

high degree of BaTiO₃ chemical bond covalency, which is typical for all ABO₃ perovskites. The bond population between Ti and O atoms in BaTiO₃ bulk is exactly the same as in PbTiO₃ bulk, namely +98me. The largest bond population between Zr and O atoms is for BaZrO₃ bulk, +108me. The smallest bond population between Ti and O atoms between all seven ABO₃ perovskites is for the CaTiO₃ bulk +84me.

The optical direct (Γ–Γ) bulk bandgaps of five ABO₃ perovskites obtained using various functionals are summarized in Table 3. This table clearly demonstrates that pure HF calculations overestimate the optical bandgap several times for all six perovskites, whereas LDA and GGA calculations by factor of approximately 1.5 underestimate it. This tendency is well known in solid state physics for all materials, for example, CaF₂ and BaF₂.^{117,119} The most realistic bandgaps for SrTiO₃, BaTiO₃, PbTiO₃, BaZrO₃, SrZrO₃ and PbZrO₃ perovskites in Refs. 25, 47, 64 and 68 have been obtained using the hybrid B3LYP and B3PW functionals, in agreement with a study by Muscat *et al.*¹⁵⁴

As we can see from Table 3, the SrTiO₃ experimental bandgap is 3.75 eV, as determined by van Benthem *et al.*¹⁵⁵ using the spectroscopic ellipsometry, 3.2 eV bandgap has been experimentally measured for BaTiO₃¹⁵⁶ and 3.4 eV for PbTiO₃.¹⁵⁷ The calculated optical bandgap for the SrTiO₃ perovskite 3.89 eV, using the B3LYP functional in Ref. 114, is in an excellent agreement with the experimental value of 3.75 eV.¹⁵⁵ Using the B3PW hybrid functional,¹¹⁴ 3.96 eV have been obtained for the SrTiO₃ bandgap. The bandgaps calculated for BaTiO₃ and PbTiO₃ crystals by means of B3LYP functional,¹¹⁴ 3.49 eV and 4.15 eV, respectively, are also in a satisfactory agreement with the experiment, the discrepancy is 22%. This is acceptable if we take into account the difficulties in determining experimentally the bandgap, including the optical absorption edge tails which extend up to several tenths of eV.⁵ The calculated forbidden optical bandgap for the SrZrO₃ crystal⁶⁸ depends considerably on the choice of the exchange–correlation functional (see Table 3). As usual,^{161,162} the HF bandgap is considerably overestimated (13.54 eV), whereas PWGGA (3.53 eV) and PBE (3.52 eV) are underestimated. The best result for the SrZrO₃ crystal are obtained for the hybrid B3LYP method.⁶⁸ Calculated optical bandgap by means of the B3LYP method,

Ab initio calculations of ABO₃ perovskite surfaces and defects

5.31 eV, is in an excellent agreement with the experimentally measured SrZrO₃ optical bandgap of 5.6 eV.¹⁶⁰

In ABO₃ perovskite (001) surface structure simulations presented in Table 4 atoms of two or three outermost surface layers were allowed to relax along the *z*-

Table 4. Calculated atomic relaxation (in percent of bulk lattice constant) for AO and BO₂-terminated ABO₃ perovskite (001) surfaces. Positive (negative) values refer to displacements outward from (inward to) the surface.

SrTiO ₃					TiO ₂					
Layer	Ion	B3PW ^a	SM ^b	LDA ^c	LDA ^d	Ion	B3PW ^a	SM ^b	LDA ^c	LDA ^d
1	Sr	-4.84	-7.10	-5.7	-6.66	Ti	-2.25	-2.96	-3.4	-1.79
	O	0.84	1.15	0.1	1.02	O	-0.13	-1.73	-1.6	-0.26
2	Ti	1.75	1.57	1.2	1.79	Sr	3.55	3.46	2.5	4.61
	O	0.77	0.87	0.0	0.26	O	0.57	-0.21	-0.5	0.77
3	Sr		-1.42	-1.2	-1.54	Ti		-0.60	-0.7	-0.26
	O		0.70	-0.1	0.26	O		-0.29	-0.5	0.26
BaTiO ₃					TiO ₂					
Layer	Ion	B3PW ^a	SM ^b	LDA ^e	Ion	B3PW ^a	SM ^b	LDA ^e		
1	Ba	-1.99	-3.72	-2.79	Ti	-3.08	-2.72	-3.89		
	O	-0.63	1.00	-1.40	O	-0.35	-0.94	-1.63		
2	Ti	1.74	1.25	0.92	Ba	2.51	2.19	1.31		
	O	1.40	0.76	0.48	O	0.38	-0.17	-0.62		
3	Ba		-0.51	0.53	Ti		-0.33	-0.75		
	O		0.16	0.26	O		-0.01	-0.35		
PbTiO ₃					TiO ₂					
Layer	Ion	B3PW ^a	LDA ^f		Ion	B3PW ^a	LDA ^f			
1	Pb	-3.82	-4.36		Ti	-2.81	-3.40			
	O	-0.31	-0.46		O	0.31	-0.34			
2	Ti	3.07	2.39		Pb	5.32	4.53			
	O	2.30	1.21		O	1.28	0.43			
3	Pb		-1.37		Ti				-0.92	
	O		-0.20		O				-0.27	
CaTiO ₃					TiO ₂					
Layer	Ion	B3PW ^g	GGA ^h		Ion	B3PW ^g	GGA ^h			
1	Ca	-8.31	-2.27		Ti	-1.71	-0.75			
	O	-0.42	0.18		O	-0.10	-0.13			
2	Ti	1.12	0.70		Ca	2.75	1.98			
	O	0.01	0.31		O	1.05	0.21			
3	Ca		-0.82		Ti		-0.23			
	O		-0.03		O		-0.23			
PbZrO ₃					ZrO ₂					
Layer	Ion	B3LYP ⁱ	B3PW ^j	LDA ^k	Ion	B3LYP ⁱ	B3PW ^j	LDA ^k		
1	Pb	-5.69	-6.95	-4.9	Zr	-2.37	-2.97	-1.9		
	O	-2.37	-0.04	1.2	O	-1.99	-1.36	-0.5		
2	Zr	0.57	2.57	2.6	Pb	4.36	5.54	4.7		
	O	0.09	1.08	0.9	O	1.04	0.84	1.1		
3	Pb	-0.47	-2.63	-1.1	Zr	-0.47	-1.12	-0.3		
	O	-0.47	-0.26	0.3	O	-0.28	-0.53	0.3		

^aReference 25.^bReference 44.^cReference 42.^dReference 41.^eReference 46.^fReference 43.^gReference 57.^hReference 58.ⁱReference 68.^jReference 61.^kReference 163.

R. I. Eglitis

axis (surfaces of perfect cubic crystals by symmetry have no forces along the x - and y -axes). A comparison of the surface atomic displacements obtained by different theoretical methods is also done in Table 4. The relaxation of surface metal atoms for SrTiO₃, BaTiO₃, PbTiO₃, CaTiO₃ and PbZrO₃ perovskite upper two surface layers is much larger than that of oxygen ions what leads to a considerable *rumpling* of the outermost plane (see Tables 4 and 5). The metal atoms of the first and third SrTiO₃, BaTiO₃, PbTiO₃, CaTiO₃ and PbZrO₃ surface layers relax inwards, i.e., toward the bulk, whereas the second layer metal atoms relax upwards. The only exception is upward relaxation of the BaO-terminated BaTiO₃ (001) surface third layer Ba atom obtained by means of the LDA calculations.⁴⁶ The CaO-terminated CaTiO₃ (001) surface first layer Ca atoms exhibit the strongest relaxation between all AO and BO₂-terminated ABO₃ perovskite (001) surface atoms. The Ca atom inward relaxation magnitude is 8.31% of the theoretical lattice constant.

In order to compare the calculated surface structures with experimental results, the surface rumpling s (the relative displacement of oxygen with respect to the metal atom in the surface layer) and the changes in interlayer distances Δd_{12} and Δd_{23} (1, 2 and 3 are the numbers of near-surface layers) are presented in Table 5. Calculations of the interlayer distances are based on the positions of relaxed metal ions, which are known to be much stronger electron scatters than oxygen ions.⁷ As

Table 5. Calculated and experimental surface rumpling s and relative displacements of the three near-surface planes for the AO- and BO₂-terminated surfaces Δd_{ij} (in percent of the lattice constant).

		AO-term			BO ₂ -term		
		s	Δd_{12}	Δd_{23}	s	Δd_{12}	Δd_{23}
SrTiO ₃	B3PW ^a	5.66	-6.58	1.75	2.12	-5.79	3.55
	LDA ^b	5.8	-6.9	2.4	1.8	-5.9	3.2
	LDA ^c	7.7	-8.6	3.3	1.5	-6.4	4.9
	SM ^d	8.2	-8.6	3.0	1.2	-6.4	4.0
	LEED ^e	4.1 ± 2	-5 ± 1	2 ± 1	2.1 ± 2	1 ± 1	-1 ± 1
	RHEED ^f	4.1	2.6	1.3	2.6	1.8	1.3
BaTiO ₃	B3PW ^g	1.37	-3.74	1.74	2.73	-5.59	2.51
	LDA ^h	1.39	-3.71	0.39	2.26	-5.2	2.06
	SM ⁱ	0.37	-2.42	2.39	1.4	-6.5	3.17
	SM ^d	4.72	4.79	1.76	1.78	-4.91	2.52
PbTiO ₃	B3PW ^g	3.51	6.89	3.07	3.12	-8.13	5.32
	LDA ^j	3.9	6.75	3.76	3.06	-7.93	5.45
CaTiO ₃	B3PW ^h	7.89	-9.43	1.12	1.61	-4.46	2.75
PbZrO ₃	LDA ^l	6.88	-8.6	3.4	1.1	-7.1	4.9
BaZrO ₃	B3PW ^m	3.07	-4.77	0.48	0.09	-3.73	1.97
	B3LYP ⁿ	6.77	-8.49	2.39	-0.72	-4.19	2.85
	LDA ^o	7.9	-9.1	3.2	-0.7	-6.1	4.2
	GGA ^o	7.8	-9.3	3.3	0.3	-7.4	4.9

^aReference 25.

^bReference 42.

^cReference 41.

^dReference 44.

^eReference 7.

^fReference 8.

^gReference 47.

^hReference 46.

ⁱReference 164.

^jReference 43.

^kReference 57.

^lReference 63.

^mReference 64.

ⁿReference 68.

^oReference 65.

Ab initio calculations of ABO₃ perovskite surfaces and defects

we can see from Table 5, nice qualitative agreement, for example for the SrTiO₃ perovskite, between all theoretical methods is observed. The amplitude of surface rumpling of SrO-terminated SrTiO₃ is predicted to be much larger than that of TiO₂-terminated SrTiO₃ surface, whereas the rumpling of BaTiO₃ TiO₂-terminated surface is predicted to exceed by a factor of two that for BaO-terminated surface. In contrast, the PbTiO₃ perovskite demonstrates practically equal rumpling for both surface terminations. From Table 5, one can see that all surfaces show the reduction of interlayer distance d_{12} and expansion of d_{23} . The calculated surface rumpling agrees quite well with LEED and RHEED experiments^{7,8} (which are available so far only for SrTiO₃ surfaces). Theory agrees qualitatively also with the LEED results for the Δd_{12} and Δd_{23} . However, the LEED and RHEED experiments demonstrate that the topmost oxygen always move outwards the surfaces whereas all calculations predict for the TiO₂-terminated SrTiO₃ surface that oxygen goes inwards. Moreover, Table 5 also shows that LEED and RHEED experiments contradict each other in the sign of Δd_{12} for SrO-terminated surface and Δd_{23} for TiO₂-terminated surface. Up to now, the reason for such discrepancies between the different experimental data is not clear and still discussed (e.g., see Ref. 42). Thus, experimental check of our predictions at the moment is prevented by a conflict between different experimental results. New detailed experimental studies are important for resolving this contradiction.

By different methods calculated surface rumpling s for SrTiO₃, BaTiO₃, PbTiO₃, CaTiO₃, BaZrO₃ and PbZrO₃ perovskite (001) surfaces was always positive (see Table 5). In contrast, the *ab initio*⁶⁸ calculated surface rumpling for the ZrO₂-terminated SrZrO₃ (001) surface is negative. Moreover, the calculated negative surface rumpling for the ZrO₂-terminated SrZrO₃ (001) surface (-0.72% of a_0) is in a surprisingly good agreement with the LDA calculation result by Wang and Arai⁶⁵ (-0.7% of a_0), however it is in contrast to the GGA result for the ZrO₂-terminated SrZrO₃ (001) surface rumpling by the same authors ($+0.3\%$ of a_0).

The calculated surface energy for the SrO-terminated SrTiO₃ (001) surface²⁵ by means of hybrid B3PW method is 1.15 eV, which is slightly smaller than the computed surface energy of 1.23 eV for the TiO₂ termination (see Table 6). The surface energies for SrTiO₃ obtained from the classical shell model⁴⁴ (1.32 eV and 1.36 eV for the SrO and TiO₂ terminations, respectively) are slightly larger. In contrast to the SrTiO₃ (001) surface, we can see that different terminations of the (011) surface lead to large differences in the surface energies. For the SrTiO₃ (011) surface, the lowest energy, according to calculations performed in Ref. 25 is 2.04 eV for the O-terminated surface. B3PW calculated surface energy of 3.06 eV for the TiO-terminated SrTiO₃ (011) surface is larger than that of the Sr-terminated (011) surface (2.66 eV). The surface energy⁹⁰ for Ti-terminated SrTiO₃ (111) surface (4.99 eV) is smaller, than the surface energy for SrO₃-terminated (111) surface (6.30 eV). The calculated surface energies of the relaxed BaTiO₃ (001) and (011) surfaces by means of the hybrid B3PW method⁴⁷ and the classical shell model⁴⁴ are

R. I. Eglitis

Table 6. Calculated surface energies (in eV per surface cell) for SrTiO₃, BaTiO₃, PbTiO₃, CaTiO₃, BaZrO₃, SrZrO₃ and PbZrO₃ (001), (011) and (111) surfaces with different terminations.

Crystal	(001)		(011)			(111)	
	AO	BO ₂	BO	A	O	AO ₃	B
SrTiO ₃	1.15 ^a	1.23 ^a	3.06 ^a	2.66 ^a	2.04 ^a	6.30 ^d	4.99 ^d
	1.32 ^b	1.36 ^b	2.21 ^b	3.04 ^b	1.54 ^b		
BaTiO ₃			2.10 ^c	2.97 ^c	1.40 ^c	8.40 ^f	7.28 ^f
	1.19 ^e	1.07 ^e	2.04 ^e	3.24 ^e	1.72 ^e		
	1.45 ^b	1.40 ^b	2.35 ^b	4.14 ^b	1.81 ^b		
PbTiO ₃	0.83 ^e	0.74 ^e	1.36 ^e	2.03 ^e	1.72 ^e		
	0.923 ^g	0.923 ^g	1.834 ^g	1.834 ^g	1.716 ^g		
CaTiO ₃	0.94 ^h	1.13 ^h	3.13 ^h	1.91 ^h	1.86 ^h	5.86 ⁱ	4.18 ⁱ
	0.824 ^j	1.021 ^j	2.180 ^j	1.671 ^j	0.837 ^j		
BaZrO ₃	1.30 ^l	1.31 ^l	3.09 ^l	2.90 ^l	2.32 ^l	9.33 ^m	7.94 ^m
PbZrO ₃	1.00 ⁿ	0.93 ⁿ	1.89 ⁿ	1.74 ⁿ	1.85 ⁿ		
SrZrO ₃	1.13 ⁿ	1.24 ⁿ	3.61 ⁿ	2.21 ⁿ	2.23 ⁿ	9.45 ^o	7.98 ^o

^aReference 25.

^bReference 44.

^cReference 84.

^dReference 90.

^eReference 47.

^fReference 91.

^gReference 165.

^hReference 57.

ⁱReference 88.

^jReference 59.

^kReference 87.

^lReference 64.

^mReference 92.

ⁿReference 68.

^oReference 93.

presented in Table 6. The B3PW calculated energies for BaO and TiO₂-terminated BaTiO₃ (001) surfaces (1.19 eV per surface cell) and (1.07 eV per surface cell) demonstrate only a small difference. Unlike the BaTiO₃ (001) surface, different terminations of the (011) surface show great differences in the surface energies, according to the calculations performed by means of the B3PW method.⁴⁷ The lowest surface energy has the O-terminated surface (1.72 eV). This is close to the energy of BaTiO₃ (001) surfaces. That means that O-terminated BaTiO₃ (011) surface and BaTiO₃ (001) surfaces can co-exist. The Ba-terminated BaTiO₃ (011) surface shows much higher surface energy of 3.24 eV, while the BaTiO₃ TiO-terminated (011) surface energy is 2.04 eV. Similarly as for the SrTiO₃ perovskite, also for BaTiO₃, the (111) surface energies are considerably larger than the (001), and even (011) surface energies. The B3LYP calculated⁹¹ surface energy for Ti-terminated BaTiO₃ (111) surface is equal to 7.28 eV, while the surface energy for BaO₃-terminated BaTiO₃ (111) surface is equal to 8.40 eV. The corresponding results are also given for the (001) and (011) surfaces of PbTiO₃ in Table 6. B3PW calculations results⁴⁷ for the PbTiO₃ (001) surfaces are qualitatively similar to those for BaTiO₃, although the relaxed surface energies are somewhat lower. For the case of the PbTiO₃ (011) surfaces, we find⁴⁷ that the surface energy for the O-terminated PbTiO₃ (011) surface is exactly the same as for the O-terminated BaTiO₃ (011) surface (1.72 eV). It is worth noting, that also the surface energy for the O-terminated PbTiO₃ (011) surface (1.716 eV) calculated 2 years later in Ref. 165 practically coincides with the O-terminated PbTiO₃ and BaTiO₃ (011) surface energy (1.72 eV), calculated in Ref. 47. The surface energies for the CaTiO₃ (001) surface⁵⁷ are quite similar at 0.94 eV and 1.13 eV, respectively for the CaO and TiO₂-terminated surfaces. In con-

Ab initio calculations of ABO₃ perovskite surfaces and defects

trast, different terminations of the (011) CaTiO₃ surface lead⁵⁷ to very different surface energies of 1.86 eV, 1.91 eV and 3.13 eV for the O-terminated, Ca-terminated and TiO-terminated (011) surface, respectively. B3PW results for CaTiO₃ (011) surface energies obtained by Eglitis and Vanderbilt in Ref. 57 contrast sharply with those of Zhang *et al.*,⁵⁹ where the authors found a rather different pattern of surface energies. Namely, Zhang *et al.*⁵⁹ found that the TiO₂-terminated CaTiO₃ (001) surface energy 1.021 eV is larger than the O-terminated CaTiO₃ (011) surface energy 0.837 eV. This result by Zhang *et al.*⁵⁹ for CaTiO₃ surfaces contrast sharply with all results of all surface energy calculations for ABO₃ perovskites, where the calculated (001) surface energies were always lower than the (011) surface energies. According to my calculations,⁶⁴ the BaZrO₃ surface energy value for the BaO termination 1.30 eV is slightly smaller than for the ZrO₂ termination 1.31 eV. However, the surface energy difference is small, and both surfaces are stable and energetically almost equally favorable. Unlike the BaZrO₃ (001) surface,⁶⁴ different terminations of the (011) surface lead to great differences in the surface energies. The lowest calculated energy is that of the O-terminated BaZrO₃ (011) surface 2.32 eV. In Ref. 64 calculated surface energy for the ZrO-terminated BaZrO₃ (011) surface 3.09 eV is larger than that for the Ba-terminated BaZrO₃ (011) surface 2.90 eV. The B3LYP calculated⁹² surface energy for Zr-terminated BaZrO₃ (111) surface is equal to 7.94 eV, while the surface energy for BaO₃-terminated (111) surface is equal to 9.33 eV.

The atomic displacements D , effective static atomic charges Q , and bond populations P between nearest metal and oxygen atoms for the SrTiO₃, BaTiO₃ and PbTiO₃ (001) surfaces are given^{25,47} in Table 7. The major effect observed here for all three SrTiO₃, BaTiO₃ and PbTiO₃ perovskites is a strengthening of the Ti–O chemical bond near the TiO₂-terminated (001) surface. It is interesting to note, that the Ti and O effective charges in bulk SrTiO₃ of $2.351e$ and $-1.407e$, in bulk BaTiO₃ of $2.367e$ and $-1.388e$ and in bulk PbTiO₃ of $2.341e$ and $-1.232e$, respectively (see Table 2), are much smaller than those expected in an ionic model ($4e$ and $-2e$, respectively). The Ti–O bond population for the TiO₂-terminated SrTiO₃ (001) surface is $0.118e$, as well as $0.126e$ and $0.114e$ for the TiO₂-terminated BaTiO₃ and PbTiO₃ (001) surfaces (see Table 7), which is considerably larger than the respective values of $0.088e$, $0.098e$ and $0.098e$ in the SrTiO₃, BaTiO₃ and PbTiO₃ bulk.^{25,47} In contrast, the Sr–O and Ba–O bond populations are very small. The lack of covalency in the Sr–O and Ba–O bonds are also seen in the Sr and Ba effective charges of $1.871e$ and $1.797e$ in the bulk and $1.846e$ and $1.752e$ on the SrO- and the BaO-terminated (001) surface, which are close to the formal ionic charge of $2e$.

The optical bandgaps for SrTiO₃, BaTiO₃, PbTiO₃, SrZrO₃ and BaZrO₃ perovskites surfaces and bulk as calculated by means of the hybrid DFT technique are presented in Table 8. One can see good agreement between the theory and experiment. We should stress here the remarkable agreement of the bulk bandgap with

R. I. Eglitis

Table 7. Calculated absolute magnitudes of atomic displacements D (in Å), the effective atomic charges Q (in e), and the bond populations P between nearest Me-O atoms (in e) for the TiO₂, SrO, BaO and PbO-terminated SrTiO₃, BaTiO₃ and PbTiO₃ (001) surfaces.

Layer	Prop	STO				BTO				PTO			
		Ion	TiO ₂	Ion	SrO	Ion	TiO ₂	Ion	BaO	Ion	TiO ₂	Ion	PbO
1	D	Ti	-0.088 ^a	Sr	-0.189	Ti	-0.123 ^b	Ba	-0.080	Ti	-0.111 ^b	Pb	-0.150
	Q		2.291		1.846		2.307		1.752		2.279		1.276
	P	O	0.118	O	-0.006	O	0.126	O	-0.030	O	0.114	O	0.054
	D		-0.005		0.033		-0.014		-0.025		0.012		-0.012
	Q		-1.296		-1.522		-1.280		-1.473		-1.184		-1.128
	P		-0.014		0.074		-0.038		0.080		0.044		0.106
2	D	Sr	0.139	Ti	0.068	Ba	0.101	Ti	0.070	Pb	0.209	Ti	0.121
	Q		1.850		2.363		1.767		2.379		1.275		2.331
	P	O	-0.008	O	0.078	O	-0.030	O	0.088	O	0.008	O	0.080
	D		0.022		0.030		0.015		0.056		0.050		0.091
	Q		-1.365		-1.450		-1.343		-1.418		-1.167		-1.258
	P		0.080		-0.010		0.090		-0.030		0.080		0.006
3	Q	Ti	2.348	Sr	1.875	Ti	2.365	Ba	1.803	Ti	2.335	Pb	1.358
	P		0.096		-0.012		0.104		-0.036		0.108		0.024
	Q	O	-1.384	O	-1.429	O	-1.371	O	-1.417	O	-1.207	O	-1.259
	P		-0.010		0.084		-0.034		0.098		0.018		0.096

^aReference 25. ^bReference 47.

Ab initio calculations of ABO₃ perovskite surfaces and defects

Table 8. Calculated optical bandgap for SrTiO₃, BaTiO₃, PbTiO₃ (001), as well as for SrZrO₃ (001) and (011) and BaZrO₃ (111) surfaces (in eV).

Term	STOgap	Term	BTOgap	Term	PTOgap	Term	SZOGap	Term	BZOGap
Exp.	3.75 ^a	Exp.	3.2 ^c	Exp.	3.4 ^d	Exp.	5.6 ^e	Exp.	5.00 ^g
Bulk	3.96 ^b	Bulk	3.55 ^b	Bulk	4.32 ^b	Bulk	5.31 ^f	Bulk	4.79 ^h
SrO (001)	3.72 ^b	BaO (001)	3.49 ^b	PbO (001)	3.58 ^b	SrO (001)	5.04 ^f	BaO ₃ (111)	4.51 ^h
TiO ₂ (001)	3.95 ^b	TiO ₂ (001)	2.96 ^b	TiO ₂ (001)	3.18 ^b	ZrO ₂ (001)	4.91 ^f	Zr (111)	4.47 ^h
						O (011)	5.27 ^f		
						Sr (011)	4.40 ^f		
						ZrO (011)	5.07 ^f		

^aReference 155. ^bReference 32. ^cReference 156. ^dReference 157. ^eReference 160. ^fReference 68. ^gReference 159.

^hReference 92.

R. I. Eglitis

the experiment for SrTiO₃ (3.96 eV versus 3.75 eV) and for BaZrO₃ (4.79 eV versus 5.00 eV). This is in a sharp contrast with the typical HF overestimate of the gap and DFT underestimate for oxide and fluoride materials^{114,119,166–168} (e.g., 1.8 eV for SrTiO₃ and BaTiO₃^{42,46}).

The optical bandgap for the SrO- and TiO₂-terminated SrTiO₃ (001) surface becomes smaller with respect to the bulk bandgap.³² In the Ref. 32 by means of the hybrid B3PW method calculated bulk optical bandgap (3.96 eV) is considerably reduced for the SrO-terminated (3.72 eV) SrTiO₃ (001) surface. In contrast, the optical bandgap for the TiO₂-terminated SrTiO₃ (001) surface (3.95 eV) is only slightly, by 0.01 eV, reduced with respect to the bulk value.³² According to the earlier LDA calculations⁴² by Padilla and Vanderbilt performed 15 years ago for the SrTiO₃ (001) surface, we see that the bandgap for the SrO-terminated surface (1.86 eV) almost does not change with respect to the bulk value (1.85 eV). For the TiO₂-terminated surface, there is a substantial reduction of the bandgap (1.13 eV).

The BaTiO₃ bulk bandgap⁴⁶ calculated by Padilla and Vanderbilt by means of the LDA method is 1.79 eV, to be compared with the experimental value of 3.2 eV; this level of disagreement is typical for the LDA. The calculated⁴⁶ LDA band structure for cubic BaO-terminated BaTiO₃ (001) surface shows, that the bulk gap (1.79 eV) is slightly increased (1.80 eV) near the BaO-terminated (001) surface. On the TiO₂-terminated BaTiO₃ (001) surface, however, the bandgap is very strongly reduced (0.84 eV).⁴⁶ According to the B3PW calculations performed in Ref. 34, the BaTiO₃ optical bulk bandgap (3.55 eV) is in a good agreement with the experimental value of (3.2 eV). The optical bandgap near the BaO-terminated (3.49 eV) and TiO₂-terminated (2.96 eV) BaTiO₃ (001) surfaces are reduced with respect to the bulk value (see Table 8). By means of the hybrid B3PW method calculated³² bulk bandgap for PbTiO₃ (4.32 eV) by 0.92 eV exceed the experimental value (3.4 eV). The calculated bandgaps³² of PbO (3.58 eV) and TiO₂ (3.18 eV) terminated PbTiO₃ (001) surface are strongly, by 0.74 eV and 1.14 eV reduced with respect to the PbTiO₃ bulk bandgap value.

We should stress here outstanding agreement of in Ref. 68 by means of the B3LYP method calculated SrZrO₃ optical bulk bandgap, 5.31 eV, with the experimental value of 5.6 eV (see Table 8). This is in a sharp contrast with the typical HF overestimate of the optical bulk bandgap, 13.54 eV, and PBE underestimate of 3.52 eV.⁶⁸ The calculated optical bandgap for the SrO (5.04 eV) and ZrO₂ (4.91 eV) terminated SrZrO₃ surfaces becomes smaller with respect to the bulk optical bandgap (5.31 eV).⁶⁸ By means of the hybrid B3LYP method calculated⁹² BaZrO₃ optical bulk band gap (4.79 eV) is very slightly underestimated by 4% (see Table 8) regarding the experimental value of (5.00 eV). The calculated optical band gap near the Zr- and BaO₃-terminated BaZrO₃ (111) surfaces is reduced by approximately 6% with respect to the bulk value. The B3LYP calculated optical bandgap values for Zr- and BaO₃-terminated BaZrO₃ (111) surfaces are very close and differ only by 0.04 eV.⁹²

Ab initio calculations of ABO₃ perovskite surfaces and defects

Table 9. Atomic relaxation of the SrTiO₃, BaTiO₃, PbTiO₃ and CaTiO₃ (011) surfaces (in percent of the bulk lattice constant) for the three terminations calculated by means of the *ab initio* B3PW method and classical SM. A positive sign corresponds to outward atomic displacements (toward the vacuum).

Layer	SrTiO ₃			BaTiO ₃			PbTiO ₃			CaTiO ₃		
	Ion	Δz	Δy	Ion	Δz	Δy	Ion	Δz	Δy	Ion	Δz	Δy
		TiO-term			TiO-term			TiO-term			TiO-term	
1	Ti	-7.69 ^a	—	Ti	-6.93 ^b	—	Ti	-8.13 ^c	—	Ti	-7.14 ^d	—
1	O	3.59	—	O	6.45	—	O	3.30	—	O	4.67	—
2	O	-0.51	—	O	-1.66	—	O	-0.41	—	O	-0.44	—
3	Sr	-2.10	—	Ba	-3.85	—	Pb	-2.54	—	Ca	-2.75	—
3	O	-2.56	—	O	-2.40	—	O	-4.07	—	O	-3.79	—
3	Ti	0.16	—	Ti	1.59	—	Ti	0.30	—	Ti	-0.78	—
		Sr-term			Ba-term			Pb-term			Ca-term	
1	Sr	-12.81 ^a	—	Ba	-13.49 ^b	—	Pb	-11.94 ^c	—	Ca	-16.05 ^d	—
2	O	1.02	—	O	2.80	—	O	-0.61	—	O	1.35	—
3	Ti	-0.04	—	Ti	-1.20	—	Ti	1.78	—	Ti	-0.37	—
3	O	-1.08	—	O	-2.94	—	O	1.67	—	O	-1.71	—
3	Sr	0.26	—	Ba	2.52	—	Pb	1.52	—	Ca	-0.93	—
		O-term			O-term			O-term			O-term	
1	O	-6.61 ^a	-0.14 ^a	O	-11.16 ^b	-6.70 ^b	O	-7.37 ^c	-0.07 ^c	O	-6.10 ^d	-2.16 ^d
2	Ti	-1.02	-4.35	Ti	-1.83	-5.33	Ti	0.20	-2.54	Ti	-0.26	-4.70
2	Sr	-1.18	0.85	Ba	4.84	-2.21	Pb	0.18	-7.50	Ca	-2.10	-0.27
2	O	1.79	6.40	O	4.54	5.90	O	0.51	2.19	O	3.43	8.05
3	O	-0.79	2.10	O	6.52	5.58	O	-0.41	3.30	O	-0.55	1.90

^aReference 25. ^bReference 44. ^cReference 47. ^dReference 57.

3.2. ABO₃ perovskite (011) and (111) surface structure

Table 9 for the SrTiO₃, BaTiO₃, PbTiO₃ and CaTiO₃ (011) surfaces is similar to Table 4 for the corresponding (001) surfaces, whereas Table 10 complements these data by the predicted surface rumpling and the relative displacements of the two top layers. For the TiO-terminated surface, the rumpling for all four SrTiO₃, BaTiO₃, PbTiO₃ and CaTiO₃ (011) surfaces is qualitatively similar and really huge, ≈ 10 –14%. For all four calculated ABO₃ perovskites, this arise due to a combination of a strong O ion outward displacement by (3–6%) and large Ti ion inward displacement by approximately (7–8%). This calculated surface rumpling is much larger than that found for the (001) surface. The reduction of relative distances between the first and second layer for TiO-terminated (011) surface for all four calculated perovskites (see Table 10) are in the range between (4%) and (7%). This reduction of interlayer distance between the first and the second layer is considerably larger than the reduction of the interlayer distance between the second and the third layer. As we can see from the Table 10, the TiO-terminated CaTiO₃ (001) surface, in contrast to SrTiO₃, BaTiO₃ and PbTiO₃ perovskites, shows expansion between the second and third layers.

On the Sr, Ba, Pb and Ca-terminated SrTiO₃, BaTiO₃, PbTiO₃ and CaTiO₃ (011) surfaces, the upper layer Sr, Ba, Pb and Ca atoms move very strongly inwards

R. I. Eglitis

Table 10. Surface rumpling s and relative displacements Δd_{ij} (in percent of the bulk lattice constant) for three near-surface planes of the TiO and O-terminated SrTiO₃, BaTiO₃, PbTiO₃ and CaTiO₃ (011) surface.

	s	TiO-term		O-term	
		Δd_{12}	Δd_{23}	Δd_{12}	Δd_{23}
SrTiO ₃					
B3PW ^a	11.28	-7.18	-0.67	-5.59	-0.23
SM ^b	14.47	-4.27	-3.86	-11.83	8.69
BaTiO ₃					
B3PW ^c	10.47	-6.84	-1.02	-5.25	-1.05
SM ^b	13.38	-5.27	-3.25	-9.33	-8.35
PbTiO ₃					
B3PW ^c	11.43	-4.83	-0.71	-7.57	-5.84
CaTiO ₃					
B3PW ^d	11.81	-6.70	2.31	-5.84	0.29

^aReference 25. ^bReference 44. ^cReference 47. ^dReference 57.

by 12.81, 13.49, 11.94 and 16.05% of the lattice constant a_0 , respectively (see Table 9). These Sr, Ba, Pb and Ca atomic displacement magnitudes are the largest atomic displacement magnitudes among all in Table 9 calculated SrTiO₃, BaTiO₃, PbTiO₃ and CaTiO₃ (011) surface atoms. The second layer O atoms for the Sr, Ba and Ca-terminated SrTiO₃, BaTiO₃ and CaTiO₃ (011) surfaces relax outwards by 1.02, 2.80 and 1.35% of a_0 , respectively, whereas the Pb-terminated PbTiO₃ (011) surface second layer O atom relax inwards by 0.61% of a_0 (see Table 9). The third layer atoms for the Sr, Ba and Ca-terminated SrTiO₃, BaTiO₃ and CaTiO₃ (011) surfaces relax inwards. The only two exceptions there are the outward movement of the Sr-terminated SrTiO₃ (011) surface third layer Sr atom (0.26%), and rather strong Ba-terminated BaTiO₃ (011) surface third layer Ba atom displacement by 2.52% of a_0 (see Table 9). In contrast to Sr, Ba and Ca-terminated SrTiO₃, BaTiO₃ and CaTiO₃ (011) surfaces, all Pb-terminated PbTiO₃ (011) surface third layer atoms relax outwards. For the O-terminated SrTiO₃, BaTiO₃, CaTiO₃ and PbTiO₃ (011) surface (see Table 9), the upper layer O atom displacement directions along the z - and y -axes are the same for all four perovskites. Nevertheless, the displacement magnitudes of the upper layer O atom are quite different for different perovskites. As we can see from Table 9, the atomic displacements in the third plane from the surface for all three terminations of the SrTiO₃, BaTiO₃, PbTiO₃ and CaTiO₃ (011) surface are still large. This is in sharp contrast to results for the neutral (001) surfaces in Table 4, where the atomic displacements converged very quickly and were already negligible in the third layer.

Table 11 shows the calculated Mulliken effective charges Q and their changes ΔQ with respect to bulk SrTiO₃, BaTiO₃, PbTiO₃ and CaTiO₃ for the three (011) terminations in Ref. 25, 47 and 57. The charge of the surface Ti atoms in the TiO-terminated SrTiO₃, BaTiO₃, PbTiO₃ and CaTiO₃ (011) surface is reduced by 0.14 e , 0.151 e , 1.129 e and 0.126 e , respectively. Metal atoms in the third layer lose much

*Ab initio calculations of ABO₃ perovskite surfaces and defects*Table 11. Calculated Mulliken atomic charges Q (in e) and changes in atomic charges ΔQ with respect to the bulk charges (in e) for the three SrTiO₃, BaTiO₃, PbTiO₃ and CaTiO₃ (011) surface terminations.

Atom	Q	ΔQ	Atom	Q	ΔQ	Atom	Q	ΔQ	Atom	Q	ΔQ			
SrTiO₃														
Ti(I)	2.211 ^a	-0.140 ^a	BaTiO ₃	TiO-term	2.216 ^b	-0.151 ^b	PbTiO ₃	Ti(I)	2.212 ^b	-0.129 ^b	CaTiO ₃	Ti(I)	2.204 ^c	-0.126 ^c
O(I)	-1.305	0.102	O(I)	-1.316	0.072	O(I)	-1.261	-0.029	O(I)	-1.290	0.081	O(I)	-1.290	0.081
O(II)	-1.160	0.247	O(II)	-1.155	0.233	O(II)	-1.057	0.175	O(II)	-1.057	0.232	O(II)	-1.139	0.232
Sr(III)	1.843	-0.028	Ba(III)	1.757	-0.04	Pb(III)	1.253	-0.101	Ca(III)	1.733	-0.049	Ca(III)	1.733	-0.049
Ti(III)	2.333	-0.018	Ti(III)	2.353	-0.014	Ti(III)	2.328	-0.013	Ti(III)	2.309	-0.021	Ti(III)	2.309	-0.021
O(III)	-1.333	0.074	O(III)	-1.299	0.089	O(III)	-1.18	0.052	O(III)	-1.302	0.069	O(III)	-1.302	0.069
O(IV)	-1.429	-0.022	O(IV)	-1.402	-0.014	O(IV)	-1.239	-0.007	O(IV)	-1.375	-0.004	O(IV)	-1.375	-0.004
Sr-term														
Sr(I)	1.766	-0.105	Ba(I)	1.636	-0.161	Pb(I)	1.122	-0.232	Ca(I)	1.676	-0.106	Ca(I)	1.676	-0.106
O(II)	-1.560	-0.153	O(II)	-1.483	-0.095	O(II)	-1.140	0.092	O(II)	-1.488	-0.117	O(II)	-1.488	-0.117
Sr(III)	1.874	0.003	Ba(III)	1.799	0.002	Pb(III)	1.340	-0.014	Ca(III)	1.781	-0.001	Ca(III)	1.781	-0.001
Ti(III)	2.362	0.011	Ti(III)	2.368	0.001	Ti(III)	2.343	0.002	Ti(III)	2.334	0.004	Ti(III)	2.334	0.004
O(III)	-1.486	-0.079	O(III)	-1.446	-0.058	O(III)	-1.277	-0.045	O(III)	-1.452	-0.081	O(III)	-1.452	-0.081
O(IV)	-1.396	0.011	O(IV)	-1.392	-0.004	O(IV)	-1.247	-0.015	O(IV)	-1.363	0.008	O(IV)	-1.363	0.008
O-term														
O(I)	-1.172	0.235	O(I)	-1.158	0.23	O(I)	-1.011	0.221	O(I)	-1.139	0.232	O(I)	-1.139	0.232
Sr(II)	1.851	-0.020	Ba(II)	1.766	-0.031	Pb(II)	1.257	-0.097	Ca(II)	1.751	-0.031	Ca(II)	1.751	-0.031
Ti(II)	2.240	-0.111	Ti(II)	2.213	-0.154	Ti(II)	2.237	-0.104	Ti(II)	2.235	-0.095	Ti(II)	2.235	-0.095
O(II)	-1.461	-0.054	O(II)	-1.452	-0.064	O(II)	-1.261	-0.029	O(II)	-1.422	-0.051	O(II)	-1.422	-0.051
O(III)	-1.394	0.013	O(III)	-1.317	0.071	O(III)	-1.215	0.017	O(III)	-1.359	0.012	O(III)	-1.359	0.012
Sr(IV)	1.867	-0.004	Ba(IV)	1.792	-0.005	Pb(IV)	1.355	0.001	Ca(IV)	1.774	-0.008	Ca(IV)	1.774	-0.008
Ti(IV)	2.332	-0.019	Ti(IV)	2.317	-0.05	Ti(IV)	2.317	-0.024	Ti(IV)	2.310	-0.020	Ti(IV)	2.310	-0.020
O(IV)	-1.433	-0.026	O(IV)	-1.407	-0.019	O(IV)	-1.233	-0.001	O(IV)	-1.398	-0.027	O(IV)	-1.398	-0.027

^aReference 25. ^bReference 47. ^cReference 57.

R. I. Eglitis

less charge, with Sr and Ti atoms losing $0.028e$ and $0.018e$, respectively in SrTiO_3 . Ba, Pb and Ca atoms lose $0.04e$, $0.101e$ and $0.049e$, as well as Ti atoms lose $0.014e$, $0.013e$ and $0.021e$ in BaTiO_3 , PbTiO_3 and CaTiO_3 perovskites, respectively (see Table 11). The SrTiO_3 , BaTiO_3 and CaTiO_3 TiO-terminated (011) surface O ions in the first, second and third layers, except the central one, also have charges that are reduced by $0.102e$, $0.247e$, and $0.074e$ for SrTiO_3 , by $0.072e$, $0.233e$ and $0.089e$ for BaTiO_3 and by $0.081e$, $0.232e$ and $0.069e$ for CaTiO_3 , respectively (i.e., they become less negative). In contrast, in all four in Table 11 analyzed perovskites, the central-layer O-ions slightly increase their charges by $0.022e$, $0.014e$, $0.007e$ and $0.004e$, respectively. The largest charge change in SrTiO_3 , BaTiO_3 , PbTiO_3 and CaTiO_3 perovskites is observed for subsurface O atoms ($0.247e$, $0.233e$, $0.175e$ and $0.232e$, respectively), which add up to contribute a large positive change of $0.494e$, $0.466e$, $0.350e$ and $0.464e$, respectively in the subsurface layer.

The analysis of the interatomic bond populations for the three possible SrTiO_3 , BaTiO_3 , PbTiO_3 and CaTiO_3 (011) surface terminations shows, that the most important effect observed here is a strong increase in the Ti–O chemical bonding near the surface as compared to already large Ti–O bonding in the bulk for all four perovskites.^{25,47,57} The most significant increase in the Ti–O chemical bonding in SrTiO_3 , BaTiO_3 , PbTiO_3 and CaTiO_3 perovskites occurs near the TiO-terminated (011) surface ($0.130e$, $0.130e$, $0.132e$ and $0.128e$, respectively), which is much stronger than the relevant Ti–O chemical bonding value near the TiO₂-terminated (001) surface ($0.118e$, $0.126e$, $0.114e$ and $0.114e$, respectively) and in the bulk ($0.088e$, $0.098e$, $0.098e$ and $0.084e$, respectively).

According to the results of the calculations for SrTiO_3 (111) surfaces,⁸⁹ the upper layer Ti atom for Ti-terminated SrTiO_3 (111) surface strongly (by 3.58% of the bulk lattice constant a_0) relaxes inwards (see Table 12). The second layer Sr

Table 12. Calculated relaxation of Ti and SrO₃-terminated SrTiO_3 (111), Zr and BaO₃-terminated BaZrO_3 (111) and Zr- and SrO₃-terminated SrZrO_3 (111) surface upper three layer atoms (as a percentage of the bulk crystal lattice constant $a_o = 3.914 \text{ \AA}$, $a_o = 4.234 \text{ \AA}$ and $a_o = 4.195 \text{ \AA}$, respectively).

SrTiO ₃			BaZrO ₃			SrZrO ₃		
Layer	Ion	Δz	Layer	Ion	Δz	Layer	Ion	Δz
	Ti-term			Zr-term			Zr-term	
1	Ti	-3.58^a	1	Zr	-8.03^b	1	Zr	-5.72^c
2	Sr	-11.24	2	Ba	-9.73	2	Sr	-11.92
2	O	1.53	2	O	0.78	2	O	0.79
3	Ti	0.26	3	Zr	-0.02	3	Zr	1.53
	SrO ₃ -term			BaO ₃ -term			SrO ₃ -term	
1	Sr	1.33^a	1	Ba	1.70^b	1	Sr	-0.74^c
1	O	-0.03	1	O	-0.57	1	O	-0.52
2	Ti	1.81	2	Zr	0.21	2	Zr	0.74
3	Sr	-0.03	3	Ba	0.71	3	Sr	-0.02
3	O	-0.26	3	O	-0.01	3	O	-0.18

^aReference 89. ^bReference 92. ^cReference 93.

Ab initio calculations of ABO₃ perovskite surfaces and defects

atom moves inwards by huge magnitude of 11.24% of a_0 , while the second layer O atom relaxes outwards by 1.53% of a_0 . Outward displacement of the third layer Ti atom is rather weak, less than 1% of a_0 . For the SrO₃-terminated SrTiO₃ (111) surface, the upper layer metal atom moves outwards by 1.33% of a_0 , but the upper layer O atom is displaced very slightly inwards by 0.03% of a_0 . The second layer Ti atom outward displacement (1.81% of a_0) is larger than the upper layer Sr atom relaxation. Both third layer Sr and O atoms move inwards by a very small magnitude (0.03% of a_0 and 0.26% of a_0), respectively (see Table 12). The calculated surface relaxation energy for Ti-terminated SrTiO₃ (111) surface (−1.66 eV) is almost five times larger, than the surface relaxation energy for SrO₃-terminated SrTiO₃ (111) surface⁸⁹ (−0.35 eV).

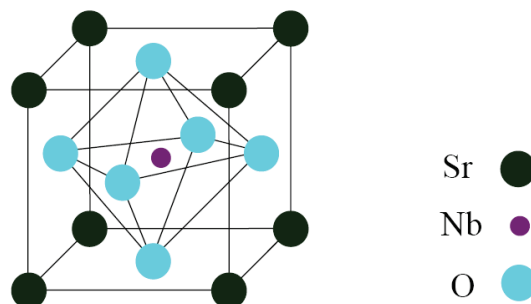
The upper layer Zr atom for Zr-terminated BaZrO₃ (111) surface strongly (by 8.03% of bulk lattice constant a_0) moves inwards toward the bulk (see Table 12).⁹² The second layer Ba atom moves inwards even more strongly (by 9.73% of a_0), while the second layer O atom relaxes slightly outwards by 0.78% of a_0 . Inward relaxation of the third layer Zr atom is very weak, only 0.02% of a_0 (see Table 12). For the BaO₃-terminated BaZrO₃ (111) surface the upper layer metal and oxygen atoms relax outwards and inwards by 1.70% of a_0 and 0.57% of a_0 , respectively.⁹² The second layer Zr atom outward relaxation magnitude (0.21% of a_0) is smaller than the third layer metal atom displacement magnitude. The calculated surface relaxation energy for Zr-terminated BaZrO₃ (111) surface (−1.49 eV) is almost fifteen times larger than the surface relaxation energy for BaO₃-terminated BaZrO₃ (111) surface (−0.10 eV).

According to the results of calculations performed in Ref. 93, the upper layer Zr atom for Zr-terminated SrZrO₃ (111) surface strongly relaxes inwards toward the bulk (by 5.72% of a_0) (see Table 12). The second layer Sr atom relaxes inwards even more strongly (by 11.92% of a_0), while the second layer O atom relaxes outwards by 0.79% of a_0 . Outward relaxation of the third layer Zr atom, similarly to the SrTiO₃ and BaZrO₃ perovskites, again is rather weak, only 1.53% of a_0 . For the SrO₃-terminated SrZrO₃ (111) surface the upper layer metal atom and oxygen atoms moves inwards by 0.74% and 0.52% of a_0 , respectively. The second layer Zr atom outward relaxation magnitude (0.74% of a_0) is exactly the same as the upper layer Sr atom inward relaxation. Both third layer Sr and O atoms relax inwards by a very small magnitude (0.02% of a_0 and 0.18% of a_0), respectively. Again, typically for ABO₃ perovskite (111) surfaces, the calculated surface relaxation energy for Zr-terminated SrZrO₃ (111) surface (−1.57 eV) is almost sixteen times larger, than the surface relaxation energy for SrO₃-terminated SrZrO₃ (111) surface⁹³ (−0.10 eV).

3.3. *Ab initio calculations of Nb impurity in SrTiO₃*

The calculated¹⁰⁶ average Sr charges in the $3 \times 3 \times 3$ times extended SrTiO₃ supercell are $1.92e$, very close to the formal ionic charge of $+2e$. This is in a sharp contrast with Ti ions ($2.77e$) and O ions ($-1.57e$), which indicates high degree of

R. I. Eglitis

Fig. 5. Sketch of Nb doped SrTiO₃ crystal.Table 13. Calculated Mulliken bond populations P (me) between different atoms in Nb doped SrTiO₃ crystal using $3 \times 3 \times 3$ times extended SrTiO₃ supercells containing 135 atoms.

Atom A	Atom B	P (me)	R (Å)
Nb	O	8 ^a	1.995
Ti	O	64	1.945
Sr	O	-22	2.751
Sr	Ti	0	3.369
Sr	Nb	0	3.369

^aReference 106.

covalency of the chemical bonding. For a single Nb ion, which replaces the Ti ion (see Fig. 5), the effective charge of $3.13e$ were found. This charge difference between the Ti and Nb ions ($0.36e$) is donated mainly to six nearest O ions which become more negative.

According to the results of our calculations, six nearest oxygen atoms are symmetrically slightly repulsed from the Nb impurity by 0.05 \AA .¹⁰⁶ It is worth noting, that Hamid in Ref. 169 using the LDA approximation got just opposite result for 6 O atoms relaxation. According to the LDA calculations by Hamid,¹⁶⁹ the six nearest O neighbors show inward relaxation toward the Nb impurity, along the $\langle 001 \rangle$ direction by 0.09 \AA . The calculated¹⁰⁶ bond populations between the nearest Ti and O atoms indicate considerable covalency effect^{170,171} (see Table 13). Just opposite, the calculated bond population between the nearest Nb and O ions turns out to be much smaller, 8 versus 64 me for the Ti–O bond. This is caused by more ionic charges of Nb and nearest O as compared to Ti and nearest O ions. The bond populations between nearest Sr and O atoms are negative which indicates the lack of chemical interaction between these ions.

The calculated HF optical bandgap is as usually strongly overestimated 12.5 eV.¹⁰⁶ The Nb impurity band in HF calculations is located 1.13 eV below the conduction band bottom. If we scale the HF calculated SrTiO₃ band gap down to the experimental value, the Nb state would be located approximately 0.25 eV

Ab initio calculations of ABO₃ perovskite surfaces and defects

below the CB bottom, which means that Nb impurity in SrTiO₃ is a shallow donor. Figure 2 in Ref. 106 shows the electronic charge density map of Nb doped SrTiO₃ bulk (the (001) plane). This figure confirms the population analysis about the covalent chemical bonding and larger effective charge of Nb ion compared to the host Ti ion.

3.4. Computer modeling of F centers in KNbO₃, PbZrO₃, SrTiO₃ and PbTiO₃

One of the most common defects in ABO₃ perovskite crystals is the so-called F center, an O vacancy V_O which traps two electrons (see Fig. 6). First principles calculations of the F centers in KNbO₃ were performed already 16 years ago by Eglitis *et al.*¹⁰⁸ using the LMTO method combined with DFT (local approximation) and the method of the INDO and relatively small 40 atom supercells. These LMTO calculations have shown for the first time that even in the ground state of the F center, the two electrons from the missing anion are considerably delocalized over the two nearest Nb ions, and only 0.6 electrons are inside the O vacancy sphere, very close to the result of INDO calculation for the relaxed structure.^{108,172–174} The INDO optimized atomic relaxation around the F center in KNbO₃ indicates a strong outward shift of the two nearest Nb neighbors with respect to the O vacancy by 6.5% of a_0 . This is accompanied by much smaller, 0.9% outward displacement of K atoms and by 1.9% inward displacement of O atoms.^{108,172–174} The two nearest Nb atoms give the largest ($\approx 80\%$) contribution to the lattice relaxation energy (3.7 eV) whereas O atoms give the most of the rest energy gain of 1 eV. The F center in KNbO₃ produces a local energy level, which lies ≈ 0.6 eV above the top of the valence band.^{108,172–174} Its molecular orbital primarily contains contribution from the atomic orbitals of the two nearest Nb atoms.

Oxygen vacancies could be created in PbZrO₃ under neutron and ionizing irradiation.¹⁷⁵ Similarly to PbTiO₃, these defects make a major impact on the overall

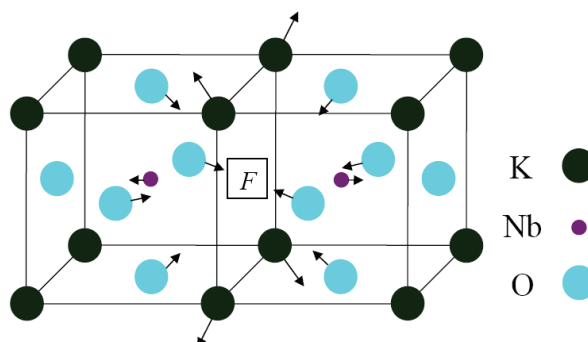


Fig. 6. Sketch of lattice relaxation around the F center in KNbO₃.

R. I. Eglitis

performance of the ferroelectric devices based on PbZrO_3 or PZT.¹⁷⁶ However, no theoretical simulations on PbZrO_3 containing defects existed until recent DFT-LCAO calculations on the atomic and electronic structure of a $3 \times 3 \times 3$ times extended supercell of cubic PbZrO_3 containing F centers.¹⁷⁷ The defect level of the F center in cubic PbZrO_3 bulk lies quite deep, 1.72 eV below the CB bottom, in the calculated bandgap of 3.78 eV.¹⁷⁸ This defect level consists mainly of $6s$ and $6p$ orbitals of the nearest Pb atoms, with a small contribution of Zr $4d$ states.¹⁷⁷ An O vacancy in the bulk PbZrO_3 attracts $0.68e$, and the remaining electron density from the missing O^{2-} is localized mostly on four nearest Pb atoms.¹⁷⁷ The two Zr atoms nearest to the defect in PbZrO_3 shift slightly outwards (by 0.48% of a_0) from the F center, while the next four Pb atoms reveal substantial displacement (5.99% of a_0) toward the F center. Deformation of the oxygen octahedra follows the displacement of Pb and Zr atoms. The F center formation energy in the PbZrO_3 bulk is equal to 7.25 eV.¹⁷⁷

The first *ab initio* calculations of oxygen vacancy on ZrO_2 -terminated PbZrO_3 (001) surface were performed by Kotomin *et al.*⁶¹ In this pilot study, the positions of all atoms surrounding the F center on the ZrO_2 terminated surface were allowed to relax. As a result, the considerable outward relaxation is observed for the two Zr atoms nearest to the oxygen vacancy (8.46% of a_0), as well as for four nearest Pb atoms (11.97% of a_0).⁶¹ The defect formation energy on the ZrO_2 terminated PbZrO_3 (001) surface containing the F center (6–7 eV) depends on the SC size and is considerably smaller than that in the PbZrO_3 bulk (7.25 eV).⁶¹ This is a driving force for the defect segregation to the PbZrO_3 surface. From the effective charge analysis, the conclusion could be drawn that only $0.3e$ is localized inside the surface oxygen vacancy, whereas the rest electron density of the missing O^{2-} ions is delocalized over the nearest atoms.⁶¹ Defect formation results in a slightly increased bandgap with respect to defectless surface structure. The surface F center band for the 3×3 surface supercell in PbZrO_3 lies in the middle of the bandgap, namely 2.58 eV below the conduction band bottom.

The F center energy level in the SrTiO_3 bulk bandgap approaches the CB bottom (being separated from it), moving from 0.69 eV for an 80-atom supercell (with the defect bandwidth of 0.15 eV), and finally reaching the optical ionization energy of 0.49 eV (with almost negligible bandwidth of 0.02–0.03 eV) for 270- and 320-atoms with the defect period close to four lattice constants.¹⁸⁰ DFT-PW calculations on 270- and 320-atom SrTiO_3 supercells give a reasonable estimate for the vacancy formation energy in the bulk, $E^{\text{form}}(F) = 7.1$ eV.¹⁷⁹ According to recent DFT-LCAO calculations on the cubic phase of SrTiO_3 perovskite by Carrasco *et al.*,¹⁸⁰ a Mulliken effective electronic charge of 1.1–1.3 e is localized inside the neutral O vacancy (depending on the supercell size) and 0.6–0.8 e are equally shared between the two nearest Ti ions. For a 320-atom SrTiO_3 bulk supercell, an expansion of the first coordination sphere (two Ti ions) (7.76% of a_0) and a compression of the second coordination sphere O atoms (7.79% of a_0) are comparable.

Ab initio calculations of ABO₃ perovskite surfaces and defects

Table 14. Comparative analysis of main properties of bulk and surface F centers in SrTiO₃, PbZrO₃, PbTiO₃ and KNbO₃ perovskites. Sign “+” corresponds to the expansion of atoms around the F center.

Property	SrTiO ₃	PbZrO ₃	PbTiO ₃	KNbO ₃
Bulk				
Charge inside V_O	1.1–1.3 ^a	0.68 ^b	0.85 ^c	0.6 ^d
F distance to CB	0.69–0.49 ^e	1.72 ^b	0.96 ^c	0.6 above the VB ^d
F formation energy	7.1 ^f	7.25 ^b	7.82 ^c	—
B relaxation	+7.76 ^f	+0.48 ^b	—	+6.5 ^d
O relaxation	–7.79 ^f	—	—	–1.9 ^d
A relaxation	+3.94 ^f	–5.99 ^b	—	+0.9 ^d
BO ₂ -term (001) surf				
Charge inside V_O	—	0.3 ^g	—	—
F distance to CB	0.25 ^e	2.58 ^g	—	—
F formation energy	6.22 ^e	6–7 ^g	—	—
B relaxation	+14 ^e	+8.46 ^g	—	—
O relaxation	–8 ^e	—	—	—
A relaxation	—	+11.97 ^g	—	—

^aReference 180. ^bReference 177. ^cReference 181. ^dReference 108.

^eReference 178. ^fReference 179. ^gReference 61.

The outward relaxation of next neighbor Sr atoms (3.94% of a_0) are almost two times smaller.¹⁷⁹

The formation energies for relaxed surface oxygen vacancy in SrTiO₃ are 6.22 eV for 120-atoms and 5.94 eV for 270-atom supercells.¹⁷⁸ The conclusion could be drawn that the defect formation energy on the TiO₂-terminated SrTiO₃ (001) surface is considerably smaller than in the SrTiO₃ bulk. The relaxation of the Ti and O atoms nearest to the surface F center are (14% of a_0) (outwards) and (8% of a_0) (mainly inwards), respectively.¹⁷⁸ The defect ionization energy of the surface F center on TiO₂-terminated SrTiO₃ (001) surface (0.25 eV) is about half that in the bulk. This is found for the 120-atom supercell, which is still far from convergence to the limit of a single defect. Here, the band dispersion is still not negligible (0.14 eV).¹⁷⁸

The defect formation energy in PbTiO₃ bulk is equal to 7.82 eV,¹⁸¹ and is approximately by 1 eV smaller than in the SrTiO₃ bulk. The F center defect level position in PbTiO₃ bulk bandgap is located 0.96 eV below the CB bottom.¹⁸¹ The Mulliken charge concentrated inside the O vacancy in PbTiO₃ bulk, according to *ab initio* calculations performed by Zhukovskii *et al.*¹⁸¹ is 0.85 e (see Table 14).

3.5. Computer modeling of hole and electron polarons in ABO₃ perovskites

A transient optical absorption band at 1.2 eV in KNbO₃ has been associated,¹⁸² in analogy with other perovskites, with a hole polaron (a hole bound, probably, to a

R. I. Eglitis

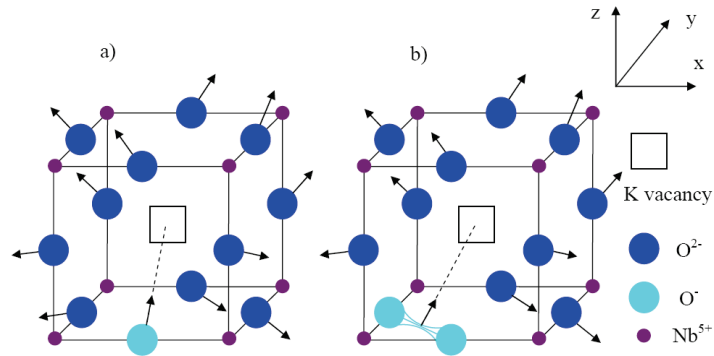


Fig. 7. Schematic view of the (a) one-site and (b) two-site hole polarons in KNbO_3 .

K vacancy) (see Fig. 7). The electron spin resonance study of KNbO_3 doped with Ti^{4+} gives a proof that holes could be trapped by such negatively charged defects.¹⁸³ The motivation for using the HF-based and DFT-based calculation methods^{184,185} simultaneously is to combine strong sides of both in a single study. The DFT is expected to be able to provide a good description of the ground state. On the other hand, the HF formalism is straightforwardly suited for the evaluation of excited energies.¹⁸⁴

The removal from the supercell of a K atom with its seven electrons contributing to the valence band (VB) produces slightly different effects on the electronic structure, as described within the DFT and the HF formalism.¹⁸⁵ In the INDO treatment, the one-electron optical gap is overestimated, as is typical for the HF calculations,¹³⁴ but the gap calculated as a difference of total energies in relaxed ground state and excited states (ΔSCF gap) gives for the triplet state 2.9 eV, close to the experiment.¹⁸⁴ The INDO calculations in contrast to the LDA suggests, that the removal of an electron leaves an unpaired electron state split off at ≈ 1 eV above the VB top.¹⁸⁴ The localized hole state is also present in the HF description but lies much lower than the corresponding state in the LDA, forming a 0.9 eV wide bandgap located ≈ 0.2 eV below the conduction band bottom.¹⁸⁵

In contrast to a generally observed large degree of covalency in KNbO_3 and contrary to a delocalized character of the F center state,^{108–110} the one-site polaron state remains well localized at the displaced O atom, with only a small contribution from atomic orbitals of other O ions but none from K or Nb ions. Despite that, there are some differences in the description of the electronic structure inside the DFT- and HF-based methods, the general trends in the total energy driving the structure optimization remain actually the same. In DFT and HF calculations,¹⁸⁴ both one-site and two-site configurations of the hole polaron are much more energetically favorable (see Table 15) than the fully symmetric relaxation of twelve O atoms around the K vacancy. This confirms what is already known about small-radius polarons in other ionic solids.^{173,186–188}

*Ab initio calculations of ABO₃ perovskite surfaces and defects*Table 15. Absorption (E_{abs}) and lattice relaxation (E_{rel} , relative to the perfect crystal with a K vacancy) energies (eV), calculated by LMTO and INDO methods.

Energy Method	E_{abs} Experiment	E_{abs} INDO	E_{rel} LMTO	E_{rel} INDO
Uniform breathing	—	—	0.01 ^b	0.08 ^b
One-site polaron	1.2 ^a	0.90 ^b	0.12 ^b	0.40 ^b
Two-site polaron	—	0.95 ^b	0.18 ^b	0.53 ^b

^aReference 182. ^bReference 184.Table 16. Optical absorption and lattice relaxation energies of electron polarons in BaTiO₃, PbTiO₃, KNbO₃ and KTaO₃ perovskites^{192–195} as calculated by means of the INDO method. Sign “+” corresponds to expansion of atoms in the x - y plane, and sign “-” corresponds to contraction of atoms in the z plane in percents of the lattice constant a_0 .

Crystal	E_{abs}	Δ in x - y plane	Δ in z plane	E_{rel}
BaTiO ₃	0.69 ^a	1.53 ^a	-1.1 ^a	0.24 ^a
PbTiO ₃	0.73 ^b	1.46 ^b	-1.04 ^b	0.22 ^b
KTaO ₃	0.75 ^c	1.70 ^c	-1.2 ^c	0.27 ^c
KNbO ₃	0.78 ^d	1.40 ^d	-1.0 ^d	0.21 ^d

^aReference 191. ^bReference 192. ^cReference 193. ^dReference 194.

The existence of small radius polarons in ionic solids was predicted by Landau in 1933.¹⁸⁶ Strict experimental (ESR) proof of self-trapped *holes* was given for alkali halides by Känzig in 1957, a quarter of century later.¹⁸⁶ In 1994, the first ESR evidence appeared¹⁸⁹ for the electron self-trapping in LiNbO₃ perovskite crystals, accompanied by the IR absorption band around 1 eV. Finally, the Nb⁴⁺ polaron absorption band around 0.72 eV has been observed recently in strontium barium niobate.¹⁹⁰

The INDO simulations for electron polarons in KNbO₃, KTaO₃, BaTiO₃ and PbTiO₃ perovskite crystals were performed,^{191–194} and the calculated energy gain due to electron self-trapping is 0.21, 0.27, 0.24 and 0.22 eV, respectively (see Table 16). The corresponding electron polaron absorption energies in KNbO₃, KTaO₃, BaTiO₃ and PbTiO₃ — 0.78, 0.75, 0.69 and 0.73 eV^{191–194} agree well with the only experimental estimate of 0.6 eV for BaTiO₃.¹⁹⁵ For example, the electron polaron in PbTiO₃ were modeled using the $3 \times 3 \times 3$ extended cubic PbTiO₃ unit cell with the LUC containing 135 atoms. In order to find the energy minimum of the system, six nearest oxygen atoms in the octahedron around a central Ti atom were allowed to relax.¹⁹² All other Ti and Pb atoms, as well as remaining O atoms, were kept fixed at their perfect lattice sites. According to INDO calculations,¹⁹² the ground state is initially three-fold degenerate (t_{2g}). This degeneracy is lifted as a result of combined breathing mode and Jahn–Teller (JT) effects: Outward displacement of

R. I. Eglitis

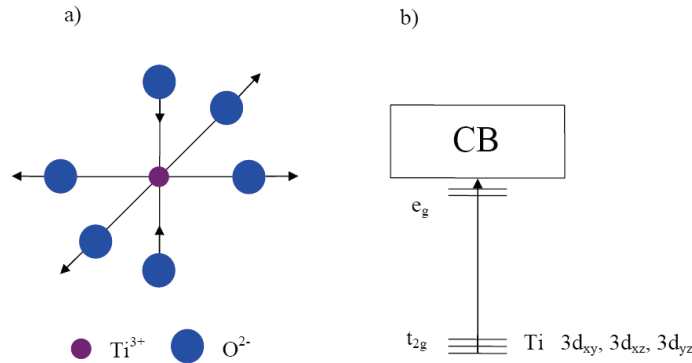


Fig. 8. (a) Sketch of the asymmetric O atom relaxations around an electron localized on the central Ti atom in the self-trapped electron in PbTiO₃. (b) Local energy states within the bandgap.

four nearest equatorial O atoms by 1.46% of a_0 and relaxation of the two oxygens inwards along the z direction by 1.04% of a_0 (see Fig. 8). The total energy gain is 0.22 eV.¹⁹² A similar JT electron polaron almost simultaneously was also observed experimentally in BaTiO₃.^{196,197}

As a result, a considerable electron density in PbTiO₃ is localized on the central Ti atom¹⁹³ producing three narrowly spaced energy levels in the bandgap. They consist mainly of the xy , xz and yz Ti 3d atomic orbitals (split t_{2g} energy level in an isolated ion); another two empty levels are located close to the conduction band bottom. The electron polaron absorption energy calculated by means of Δ SCF method is 0.73 eV.¹⁹² The absorption process corresponds to a charge transfer to the nearest Ti atom.

3.6. Computer modeling of $\text{KNb}_x\text{Ta}_{1-x}\text{O}_3$ solid solutions

Figure 4 in Ref. 198 shows the total energy curve for a 135-atom KTaO₃ cluster doped with Nb modeling an isolated Nb impurity as a function of its [111] off-center displacement. The calculated displacement of 0.146 Å by Eglitis *et al.*^{198–201} is very close to the experimental XAFS finding at 70 K.⁹⁵ The relevant energy gain is very small, only 0.0375 eV, which is a typical value for a Nb atom displacement as calculated earlier for different ferroelectric phases of KNbO₃.¹³⁴

In order to calculate the Nb cluster (see Fig. 9) in the KTaO₃ matrix Eglitis *et al.*^{198–201} have extended the primitive KTaO₃ unit cell by $4 \times 4 \times 4$, i.e., to 64 times its size, which is equivalent to carrying out the band structure calculations at 64 k -points in the Brillouin zone. In order to study the cooperative displacements (self-ordering) of Nb impurities in KTaO₃, seven Ta atoms were replaced by seven Nb atoms (see Fig. 10).

As a next step, in order to find the energy minimum of the seven atom Nb clusters in KTaO₃ matrix, six Nb atoms were allowed to relax symmetrically toward the central Nb atom. The positions of the K, Ta and O atoms were kept fixed. The

Ab initio calculations of ABO_3 perovskite surfaces and defects

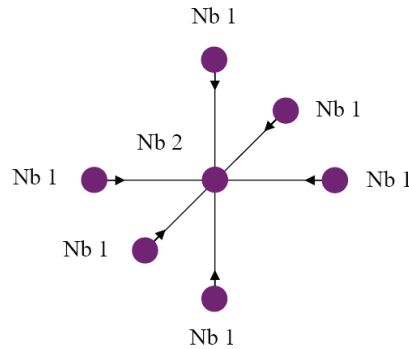


Fig. 9. Nb cluster containing seven Nb atoms inside $KTaO_3$ matrix.

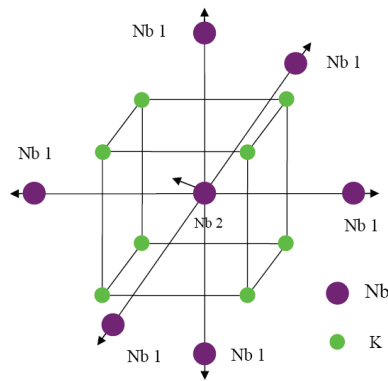


Fig. 10. Sketch of the symmetric repulsion of six Nb atoms outwards from the central Nb atom, which, as a consequence, is off-center them in both $[100]$ and $[111]$ directions.

results of numerical calculations show that six Nb atoms are displaced inwards toward the central Nb atom by 0.187 \AA , lowering the total energy of the system by 0.088 eV . However, INDO calculations show that symmetric displacements of six Nb atoms outwards by 0.073 \AA from the central Nb atom, lowering the total energy of the system by 0.03 eV , are also energetically favorable. In the case, when six Nb atoms are shifted outwards from the central Nb atom, the central Nb atom undergoes an off-center displacement from the on-site position in the $[111]$ direction by 0.27 \AA , and this is followed by an additional total energy gain of 0.09 eV — to give a total energy reduction of 0.12 eV .^{99,102}

The central Nb atom reveals instability also in the $[100]$ direction. The shift of the central Nb ion in the $[100]$ direction by 0.192 \AA additionally lowers the cluster energy by 0.056 eV , in the case when six Nb atoms are shifted outwards from the central Nb atom — to give a total energy reduction by 0.086 eV . Nevertheless, the total cluster structure induced energy lowering in the ground state, which corresponds to the situation in which six Nb atoms are symmetrically relaxed outwards

R. I. Eglitis

from the center of the Nb cluster, and the central Nb atom is displaced away from the center in the [111] direction (0.12 eV), is energetically more favorable.

According to the calculations performed by Eglitis *et al.*,^{198,201} in the case when six Nb atoms are in the energy minimum state arising from a symmetric shift of six Nb atoms towards the central Nb atom (which could be treated as an excited state of the Nb cluster), the central Nb atom exhibits on-site properties.

4. Conclusions

In this paper, the present state-of-the-art in theoretical simulations of the ABO₃ perovskite surfaces and defects therein using (mostly) first principles modeling were illustrated. According to all calculations (see Table 4), on the AO-terminated (001) surface, all upper-layer A atoms relax inward for SrTiO₃, BaTiO₃, PbTiO₃, CaTiO₃ and PbZrO₃ perovskites by magnitude of at least 2% of the lattice constant a_0 , while all second layer atoms relax outwards. For the BO₂-terminated SrTiO₃, BaTiO₃, PbTiO₃, CaTiO₃ and PbZrO₃ (001) surface, in most cases, the largest relaxations are on the second-layer metal atoms. For almost all ABO₃ perovskites, the (001) surface rumpling is much larger for the AO-terminated than for the BO₂-terminated (001) surface, but their surface energies are always quite similar.

In contrast, different terminations of the (011) ABO₃ surface lead to very different surface energies for the O-terminated, A-terminated, and BO-terminated (011) surface, respectively. A considerable increase in Ti–O or Zr–O, respectively, chemical bond covalency near the (011) surface as compared both to the bulk and to the (001) surface in ABO₃ perovskites were predicted.

For both B and AO₃-terminated SrTiO₃, BaZrO₃ and SrZrO₃ (111) surfaces the upper layer atoms, with the exception of the BaO₃ and SrO₃-terminated surface Ba and Sr atoms, respectively, relax inwards. For SrTiO₃, BaZrO₃ and SrZrO₃ (111) surfaces, the second layer Sr, Ba and Sr atoms exhibits the strongest relaxation between all atoms by 11.24, 9.73 and 11.92% of the lattice constant a_0 , respectively. The most energetically favorable with the lowest surface energy, according to all performed calculations for all perovskites, always are the AO and BO₂-terminated ABO₃ perovskite (001) surfaces. The only exception is work by Zhang *et al.*,⁵⁹ where the O-terminated CaTiO₃ (011) surface is lower in energy than the TiO₂-terminated CaTiO₃ (001) surface. The A, BO and O-terminated ABO₃ perovskite (011) surfaces are always, according to all *ab initio* and shell model calculations, less energetically favorable than (001) surfaces. Finally, the ABO₃ perovskite (111) surfaces are always energetically most unfavorable and unstable surfaces according to all performed calculations.

Calculations performed in Ref. 106 demonstrate that Nb ions substituting for host Ti ions in SrTiO₃ are shallow donors. The symmetrical outward relaxation of six nearest O ions around the Nb impurity in SrTiO₃ crystal are very small.¹⁰⁶ In the Nb doped SrTiO₃ crystal negligible chemical bonding occurs between Nb and nearest O ions. It is interesting to notice, that recent studies for the another impurity,

Ab initio calculations of ABO₃ perovskite surfaces and defects

namely the Fe impurity in the SrTiO₃ crystal bulk¹⁷⁰ and on the surface¹⁷¹ show that this is an acceptor. This demonstrates that the first-principles calculations are a reliable tool for studying the defects in perovskite materials.

A large amount of numerical calculations of mostly neutral bulk and surface oxygen vacancies performed so far for SrTiO₃, PbTiO₃, PbZrO₃ and KNbO₃ perovskites dealt with the local atomic structure and electronic density redistribution around defects in their regular lattice sites mainly after total or partial optimization of the defective structure geometry. All the calculation results for F centers in ABO₃ perovskites are in sharp contrast with what is known about F centers in ionic crystals (in particular, in MgO and alkali halides²⁰²) where the two electrons are well localized by the V_0 in the F center ground state. Obviously, this discrepancy arises from a considerable degree of covalency of the chemical bonding in ABO₃ perovskites. Electron defects (F centers) similar to what were observed in ABO₃ perovskites are known, for example, in partly covalent SiO₂ crystals (e.g., in the so-called E'_1 center an electron is also not localized inside V_0 but its wave function mainly overlaps with the sp^3 orbital centered on the neighboring Si atom²⁰³).

The quantitative models of hole polarons in KNbO₃ were analyzed.¹⁸⁴ The main conclusion is that both one-center and two-center hole polaron configurations in KNbO₃ are energetically favorable and close in energy. The calculated optical absorption energies and the spatial distribution of relevant electronic states could provide guidelines for more direct experimental identification of the defects in question. By means of the HF method calculated hole polaron absorption energy (≈ 1 eV) is close to the experimentally observed short-lived absorption band energy.¹⁸²

The quantum chemical INDO calculations^{191–194} gave additional evidence for the existence of electron polarons in BaTiO₃, KNbO₃, KTaO₃ and PbTiO₃ crystals. The theoretically calculated electron polaron absorption energy in BaTiO₃ (0.69 eV), KNbO₃ (0.78 eV), KTaO₃ (0.75 eV) and PbTiO₃ (0.73 eV) is close to the only experimental estimate of 0.6 eV for BaTiO₃.¹⁹⁵ The INDO calculated electron polaron absorption energies in KNbO₃, KTaO₃, BaTiO₃ and PbTiO₃ perovskites are smaller than the calculated and experimentally observed hole polaron absorption energies in KNbO₃. The electron polaron relaxation energies for KNbO₃, BaTiO₃, PbTiO₃ and KTaO₃ crystals are in the range from 0.21 eV till 0.27 eV.

The calculated magnitude of single Nb displacement (0.146 Å) in KTaO₃ matrix along the [111] direction is very close to the experimental XAFS finding of 0.145 Å observed at 70 K.⁹⁵ The interpretation of impurity-induced ferroelectric phase transition in terms of weak off-center impurities (like Nb⁵⁺ impurities in incipient ferroelectric KTaO₃) had been suggested on the basis of the so-called self-ordered cluster model.^{198–201} The main prediction of this model is that self-ordered clusters of the second component (Nb in KTaO₃) will form, which indeed were observed in calculations. Such self-ordered clusters of the second component in solid solutions based on ferroelectric perovskites have their own degrees of freedom. The percolation of the corresponding local order parameters as well as dynamical perco-

R. I. Eglitis

lation of the soft, low-frequency local vibrations can lead to a cooperative behavior which finally induces a ferroelectric phase transition.^{198–201}

Acknowledgments

This work was supported by the Latvian Council of Science Grant No. 374/2012 and ESF Grant No. 2013/0046/1DP/1.1.1.2.0/13/APIA/VIAA/021. The author is greatly indebted to D. Vanderbilt, K. M. Rabe, R. E. Cohen, M. R. Philpott, E. A. Kotomin, G. Borstel, J. Maier, R. Merkle, J. T. Devreese, N. E. Christensen, E. Heifets, A. V. Postnikov, D. Fuks, M. Rohlfing and S. Piskunov for fruitful discussions.

References

1. J. F. Scott, *Ferroelectric Memories* (Springer, Berlin, 2000).
2. M. Dawber, K. M. Rabe and J. F. Scott, *Rev. Mod. Phys.* **77**, 1083 (2005).
3. R. E. Cohen, *Nat. (London)* **358**, 136 (1992).
4. C. Noguera, *Physics and Chemistry at Oxide Surfaces* (Cambridge University Press, New York, 1996).
5. M. E. Lines and A. M. Glass, *Principles and Applications of Ferroelectrics and Related Materials* (Clarendon, Oxford, 1977).
6. O. Auciello, J. F. Scott and R. Ramesh, *Phys. Today* **51**, 22 (1998).
7. N. Bickel, G. Schmidt, K. Heinz and K. Müller, *Phys. Rev. Lett.* **62**, 2009 (1989).
8. T. Hikita, T. Hanada, M. Kudo and M. Kawai, *Surf. Sci.* **287–288**, 377 (1993).
9. A. Ikeda, T. Nishimura, T. Morishita and Y. Kido, *Surf. Sci.* **433–435**, 520 (1999).
10. G. Charlton *et al.*, *Surf. Sci.* **457**, L376 (2000).
11. P. A. W. Van der Heide, Q. D. Jiang, Y. S. Kim and J. W. Rabalais, *Surf. Sci.* **473**, 59 (2001).
12. W. Maus-Friedrichs *et al.*, *Surf. Sci.* **515**, 499 (2002).
13. J. A. Enterkin *et al.*, *Nat. Mater.* **9**, 245 (2010).
14. H. Bando, Y. Aiura, Y. Haruyama, T. Shimizu and Y. Nishihara, *J. Vac. Sci. Technol. B* **13**, 1150 (1995).
15. K. Szot and W. Speier, *Phys. Rev. B* **60**, 5909 (1999).
16. J. Brunen and J. Zegenhagen, *Surf. Sci.* **389**, 349 (1997).
17. Q. D. Jiang and J. Zegenhagen, *Surf. Sci.* **425**, 343 (1999).
18. J. Zegenhagen, T. Haage and Q. D. Jiang, *Appl. Phys. A* **67**, 711 (1998).
19. R. Souda, *Phys. Rev. B* **60**, 6068 (1999).
20. Y. Adachi, S. Kohiki, K. Wagatsuma and M. Oku, *J. Appl. Phys.* **84**, 2123 (1998).
21. H. Tanaka and T. Kawai, *Surf. Sci.* **365**, 437 (1996).
22. J. Chang, Y. S. Park and S. K. Kim, *Appl. Phys. Lett.* **92**, 152910 (2008).
23. S. Kimura, J. Yamauchi, M. Tsukada and S. Watanabe, *Phys. Rev. B* **51**, 11049 (1995).
24. Z. Q. Li, J. L. Zhu, C. Q. Wu, Z. Tang and Y. Kawazoe, *Phys. Rev. B* **58**, 8075 (1998).
25. R. I. Eglitis and D. Vanderbilt, *Phys. Rev. B* **77**, 195408 (2008).
26. R. Herger *et al.*, *Phys. Rev. Lett.* **98**, 076102 (2007).
27. N. Erdman *et al.*, *Nat. (London)* **419**, 55 (2002).
28. T. Kubo and H. Nozoye, *Surf. Sci.* **542**, 177 (2003).
29. E. Heifets *et al.*, *Phys. Rev. B* **64**, 235417 (2001).

Ab initio calculations of ABO₃ perovskite surfaces and defects

30. E. Heifets *et al.*, *Surf. Sci.* **513**, 211 (2002).
31. K. Johnston *et al.*, *Phys. Rev. B* **70**, 085415 (2004).
32. R. I. Eglitis *et al.*, *Ceram. Int.* **30**, 1989 (2004).
33. R. I. Eglitis *et al.*, *J. Electroceram.* **16**, 289 (2006).
34. S. Piskunov *et al.*, *Surf. Sci.* **575**, 75 (2005).
35. G. Borstel *et al.*, *Phys. Stat. Sol. B* **236**, 253 (2003).
36. R. Herger *et al.*, *Phys. Rev. B* **76**, 195435 (2007).
37. G. Borstel *et al.*, *J. Cryst. Growth* **237**, 687 (2002).
38. C. H. Lanier *et al.*, *Phys. Rev. B* **76**, 045421 (2007).
39. E. A. Kotomin, R. I. Eglitis, J. Maier and E. Heifets, *Thin Solid Films* **400**, 76 (2001).
40. Y. Li *et al.*, *Phys. Rev. B* **73**, 184112 (2006).
41. C. Cheng, K. Kunc and M. H. Lee, *Phys. Rev. B* **62**, 10409 (2000).
42. J. Padilla and D. Vanderbilt, *Surf. Sci.* **418**, 64 (1998).
43. B. Meyer, J. Padilla and D. Vanderbilt, *Faraday Discuss.* **114**, 395 (1999).
44. E. Heifets, E. A. Kotomin and J. Maier, *Surf. Sci.* **462**, 19 (2000).
45. V. Ravikumar, D. Wolf and V. P. Dravid, *Phys. Rev. Lett.* **74**, 960 (1995).
46. J. Padilla and D. Vanderbilt, *Phys. Rev. B* **56**, 1625 (1997).
47. R. I. Eglitis and D. Vanderbilt, *Phys. Rev. B* **76**, 155439 (2007).
48. F. Cora and C. R. A. Catlow, *Faraday Discuss.* **114**, 421 (1999).
49. L. Fu, E. Yaschenko, L. Resca and R. Resta, *Phys. Rev. B* **60**, 2697 (1999).
50. B. Meyer and D. Vanderbilt, *Phys. Rev. B* **63**, 205426 (2001).
51. C. Bungaro and K. M. Rabe, *Phys. Rev. B* **71**, 035420 (2005).
52. M. Krcmar and C. L. Fu, *Phys. Rev. B* **68**, 115404 (2003).
53. Y. Umeno, T. Shimada, T. Kitamura and C. Elsasser, *Phys. Rev. B* **74**, 174111 (2006).
54. R. I. Eglitis, *Integr. Ferroelectr.* **108**, 11 (2009).
55. B. K. Lai *et al.*, *Phys. Rev. B* **75**, 085412 (2007).
56. E. Heifets *et al.*, *J. Phys.: Condens. Matter* **10**, L347 (1998).
57. R. I. Eglitis and D. Vanderbilt, *Phys. Rev. B* **78**, 155420 (2008).
58. Y. X. Wang, M. Arai, T. Sasaki and C. L. Wang, *Phys. Rev. B* **73**, 035411 (2006).
59. J. M. Zhang, J. Cui, K. W. Xu, V. Ji and Z. Y. Man, *Phys. Rev. B* **76**, 115426 (2007).
60. A. Munkholm *et al.*, *Phys. Rev. Lett.* **88**, 016101 (2002).
61. E. A. Kotomin *et al.*, *Phys. Chem. Chem. Phys.* **10**, 4258 (2008).
62. R. I. Eglitis, *Integr. Ferroelectr.* **123**, 26 (2011).
63. Y. X. Wang *et al.*, *Surf. Sci.* **585**, 75 (2005).
64. R. I. Eglitis, *J. Phys.: Condens. Matter* **19**, 356004 (2007).
65. Y. X. Wang and M. Arai, *Surf. Sci.* **601**, 4092 (2007).
66. G. Pilania *et al.*, *J. Mater. Sci.* **44**, 5249 (2009).
67. R. A. Evarestov, A. V. Bandura and V. E. Alexandrov, *Phys. Stat. Sol. B* **243**, 2756 (2006).
68. R. I. Eglitis and M. Rohlfing, *J. Phys.: Condens. Matter* **22**, 415901 (2010).
69. A. Hofer *et al.*, *Phys. Rev. Lett.* **108**, 087602 (2012).
70. M. Stengal, *Phys. Rev. B* **84**, 205432 (2011).
71. R. A. Evarestov, A. V. Bandura and V. E. Alexandrov, *Surf. Sci.* **601**, 1844 (2007).
72. D. Li *et al.*, *Nat. Mater.* **7**, 473 (2008).
73. A. M. Kolpak *et al.*, *Phys. Rev. Lett.* **101**, 036102 (2008).
74. M. G. Brik, C. G. Ma and V. Krasnenko, *Surf. Sci.* **608**, 146 (2013).

R. I. Eglitis

75. J. A. Enterkin, A. E. Becerra-Toledo, K. R. Poeppelmeier and L. D. Marks, *Surf. Sci.* **606**, 344 (2012).
76. M. S. J. Marshall *et al.*, *Phys. Rev. B* **86**, 125416 (2012).
77. J. Ho, E. Heifets and B. Merinov, *Surf. Sci.* **601**, 490 (2007).
78. X. Wang, S. Tomado, T. Shimada and T. Kitamura, *Physica B* **410**, 22 (2013).
79. R. A. Evarestov, A. V. Bandura and D. D. Kuruch, *J. Comput. Chem.* **34**, 175 (2013).
80. J. He, G. B. Stephenson and S. M. Nakhmanson, *J. Appl. Phys.* **112**, 054112 (2012).
81. X. Wang, S. Tomoda, T. Shimada and T. Kitamura, *J. Phys.: Condens. Matter* **24**, 045903 (2012).
82. J. Wang, G. Tang and X. S. Wu, *Phys. Stat. Sol. B* **249**, 796 (2012).
83. F. Bottin, F. Finocchi and C. Noguera, *Phys. Rev. B* **68**, 035418 (2003).
84. E. Heifets *et al.*, *Phys. Rev. B* **69**, 035408 (2004).
85. E. Heifets, J. Ho and B. Merinov, *Phys. Rev. B* **75**, 155431 (2007).
86. A. Pojani, F. Finocchi and C. Noguera, *Surf. Sci.* **442**, 179 (1999).
87. W. Liu, C. Wang, J. Cui and Z. Y. Man, *Solid State Commun.* **149**, 1871 (2009).
88. R. I. Eglitis, *Ferroelectrics* **424**, 1 (2011).
89. R. I. Eglitis and M. Rohlfing, to appear in *Phys. Stat. Sol. B*, doi:10.1002/pssb.201248072.
90. R. I. Eglitis, *ab initio* calculations of SrTiO₃ (111) surfaces, *Proc. NATO ARW "Nanodevices and Nanomaterials for Ecological Security"*, eds. Y. N. Shunin and A. E. Kiv (Springer, Dordrecht, 2012), p. 125.
91. R. I. Eglitis, *Phase Trans.* **86**, 1115 (2013).
92. R. I. Eglitis, *Solid State Ion.* **230**, 43 (2013).
93. R. I. Eglitis, *Ferroelectrics* **436**, 5 (2012).
94. P. Günter and J. P. Huignard, *Photorefractive Materials and Their Applications*, Vols. 61–62 (Springer, Berlin, 1988).
95. O. Hanske-Petitpierre *et al.*, *Phys. Rev. B* **44**, 6700 (1991).
96. R. Niemann *et al.*, *J. Phys.: Condens. Matter* **8**, 5837 (1996).
97. P. Blennow *et al.*, *Solid State Ionics* **179**, 2047 (2008).
98. R. I. Eglitis and G. Borstel, *Phys. Stat. Sol. A* **202**, R13 (2005).
99. K. Szot *et al.*, *Nat. Mater.* **5**, 312 (2006).
100. I. Szafraniak *et al.*, *Appl. Phys. Lett.* **83**, 2211 (2003).
101. C. Binnig *et al.*, *Phys. Rev. Lett.* **45**, 352 (1980).
102. M. Takizawa *et al.*, *Phys. Rev. B* **79**, 113103 (2009).
103. R. Astala and P. D. Bristowe, *J. Phys.: Condens. Matter* **14**, L149 (2002).
104. A. S. Hamid, *Appl. Phys. A* **97**, 829 (2009).
105. X. G. Guo *et al.*, *Phys. Lett. A* **317**, 501 (2003).
106. R. I. Eglitis and E. A. Kotomin, *Physica B* **405**, 3164 (2010).
107. Y. Chen and M. M. Abraham, *J. Phys. Chem. Sol.* **51**, 747 (1990).
108. R. I. Eglitis *et al.*, *Phys. Rev. B* **56**, 8599 (1997).
109. H. Donnerberg and A. Birkholz, *J. Phys.: Condens. Matter* **12**, 8239 (2000).
110. E. A. Kotomin, R. I. Eglitis and A. I. Popov, *J. Phys.: Condens. Matter* **9**, L315 (1997).
111. V. R. Saunders *et al.*, *CRYSTAL2003 Users Manual* (University of Torino, Torino, 2003).
112. R. E. Cohen, *J. Phys. Chem. Solids* **57**, 1393 (1996).
113. R. E. Cohen, *Ferroelectrics* **194**, 323 (1997).
114. S. Piskunov *et al.*, *Comput. Mater. Sci.* **29**, 165 (2004).
115. R. Jia *et al.*, *Comput. Mater. Sci.* **73**, 9 (2013).

Ab initio calculations of ABO₃ perovskite surfaces and defects

116. L. Yue *et al.*, *J. Phys. Chem. A* **114**, 8444 (2010).
117. H. Shi, R. Jia and R. I. Eglitis, *Phys. Rev. B* **81**, 195101 (2010).
118. H. Shi, R. I. Eglitis and G. Borstel, *J. Phys.: Condens. Matter* **19**, 056007 (2007).
119. H. Shi, R. I. Eglitis and G. Borstel, *J. Phys.: Condens. Matter* **18**, 8367 (2006).
120. R. I. Eglitis, H. Shi and G. Borstel, *Surf. Rev. Lett.* **13**, 149 (2006).
121. H. Shi, R. Jia and R. I. Eglitis, *Solid State Ionics* **187**, 1 (2011).
122. H. Shi, L. Chang, R. Jia and R. I. Eglitis, *J. Phys. Chem. C* **116**, 6392 (2012).
123. H. Shi, L. Chang, R. Jia and R. I. Eglitis, *J. Phys. Chem. C* **116**, 4832 (2012).
124. H. Shi, R. I. Eglitis and G. Borstel, *Comput. Mater. Sci.* **39**, 430 (2007).
125. A. D. Becke, *J. Chem. Phys.* **98**, 5648 (1993).
126. J. P. Perdew and Y. Wang, *Phys. Rev. B* **33**, 8800 (1986).
127. J. P. Perdew and Y. Wang, *Phys. Rev. B* **40**, 3399 (1989).
128. J. P. Perdew and Y. Wang, *Phys. Rev. B* **45**, 13244 (1992).
129. H. J. Monkhorst and J. D. Pack, *Phys. Rev. B* **13**, 5188 (1976).
130. C. Pisani (ed.), *Quantum-Mechanical Ab initio Calculations of the Properties of Crystalline Materials, Lecture Notes in Chemistry* Vol. 67 (Springer, Berlin, 1996).
131. A. Pojani, F. Finocchi and C. Noguera, *Appl. Surf. Sci.* **142**, 177 (1999).
132. A. Shluger, *Theoret. Chim. Acta* **66**, 355 (1985).
133. E. Stefanovich, E. Shidlovskaya, A. Shluger and M. Zakharov, *Phys. Stat. Sol. B* **160**, 529 (1990).
134. R. I. Eglitis, A. V. Postnikov and G. Borstel, *Phys. Rev. B* **54**, 2421 (1996).
135. M. Causa and A. Zupan, *Chem. Phys. Lett.* **220**, 145 (1994).
136. K. H. Hellwege and A. M. Hellwege (eds.), *Ferroelectrics and Related Substances*, Landolt-Bornstein, New Series Vol. 3 (Springer-Verlag, Berlin, 1969).
137. R. O. Bell and G. Rupprecht, *Phys. Rev.* **129**, 90 (1963).
138. G. J. Fischer, Z. Wang and S. Karato, *Phys. Chem. Miner.* **20**, 97 (1993).
139. B. G. Shirane and R. Repinsky, *Acta Cryst.* **9**, 131 (1956).
140. Z. Li, M. Grimsditch, C. M. Foster and S. K. Chan, *J. Phys. Chem. Solids* **57**, 1433 (1996).
141. B. J. Kennedy, C. J. Howard and B. C. Chakoumakos, *J. Phys.: Condens. Matter* **11**, 1479 (1999).
142. E. Cockayne and B. P. Burton, *Phys. Rev. B* **62**, 3735 (2000).
143. J. W. Bennett, I. Grinberg and A. M. Rappe, *Phys. Rev. B* **73**, 180102R (2006).
144. R. D. King-Smith and D. Vanderbilt, *Phys. Rev. B* **49**, 5828 (1994).
145. M. E. Björketun, P. G. Sundell and G. Wähnström, *Phys. Rev. B* **76**, 054307 (2007).
146. S. Piskunov *et al.*, *Comput. Mater. Sci.* **41**, 195 (2007).
147. S. S. N. Bharadwaja and S. B. Krupanidhi, *J. Appl. Phys.* **89**, 4541 (2001).
148. P. Ghosez, E. Cockayne, U. V. Wagemare and K. M. Rabe, *Phys. Rev. B* **60**, 836 (1999).
149. A. J. Smith and A. J. Welch, *Acta Crystallogr.* **13**, 653 (1960).
150. Z. Feng, H. Hu, S. Cui and C. Bai, *Solid State Commun.* **148**, 472 (2008).
151. R. Vali, *J. Phys. Chem. Solids* **69**, 876 (2008).
152. C. R. A. Catlow and A. M. Stoneham, *J. Phys. C* **16**, 4321 (1983).
153. R. C. Bochiccio and H. F. Reale, *J. Phys. B* **26**, 4871 (1993).
154. J. Muscat, A. Wander and N. M. Harrison, *Chem. Phys. Lett.* **342**, 397 (2001).
155. K. van Benthem, C. Elsasser and R. H. French, *J. Appl. Phys.* **90**, 6156 (2001).
156. S. H. Wemple, *Phys. Rev. B* **2**, 2679 (1970).
157. C. H. Peng, J. F. Chang and S. Desu, *Mater. Res. Soc. Symp. Proc.* **243**, 21 (1992).
158. Y. X. Wang, M. Arai and T. Sasaki, *Appl. Phys. Lett.* **88**, 091909 (2006).
159. O. Fursenko *et al.*, *Thin Solid Films* **520**, 4532 (2012).

R. I. Eglitis

160. Y. S. Lee *et al.*, *Phys. Rev. B* **67**, 113101 (2003).
161. M. Catti *et al.*, *J. Phys.: Condens. Matter* **3**, 4151 (1991).
162. M. Verstraete and X. Gonze, *Phys. Rev. B* **68**, 195123 (2003).
163. Y. X. Wang, *Phys. Status Solidi B* **244**, 602 (2007).
164. S. Tinte and M. D. Stachiotti, *AIP Conf. Proc.* **535**, 273 (2000).
165. J. M. Zhang, Q. Pang, K. W. Xu and V. Ji, *Comput. Mater. Sci.* **44**, 1360 (2009).
166. A. F. Fix *et al.*, *Phys. Scr.* **86**, 035304 (2012).
167. A. F. Vassilyeva, *Physica B* **405**, 2125 (2010).
168. H. Shi, L. Chang, R. Jia and R. I. Eglitis, *Comput. Mater. Sci.* **79**, 527 (2013).
169. A. S. Hamid, *Appl. Phys. A* **97**, 829 (2009).
170. R. A. Evarestov, S. Piskunov, E. A. Kotomin and G. Borstel, *Phys. Rev. B* **67**, 064101 (2003).
171. V. Alexandrov, R. A. Evarestov, E. A. Kotomin and J. Maier, *J. Phys. Conf. Ser.* **117**, 012001 (2008).
172. R. I. Eglitis, E. A. Kotomin and G. Borstel, *Comput. Mater. Sci.* **30**, 376 (2004).
173. E. A. Kotomin, R. I. Eglitis and G. Borstel, *Comput. Mater. Sci.* **17**, 290 (2000).
174. E. A. Kotomin *et al.*, *Comput. Mater. Sci.* **10**, 339 (1998).
175. R. Bittner *et al.*, *J. Appl. Phys.* **96**, 3239 (2004).
176. C. H. Ahn *et al.*, *Appl. Phys. Lett.* **70**, 206 (1997).
177. S. Piskunov *et al.*, *Comput. Mater. Sci.* **41**, 195 (2007).
178. J. Carrasco *et al.*, *Phys. Rev. B* **73**, 064106 (2006).
179. R. A. Evarestov, E. A. Kotomin and Y. F. Zhukovskii, *Int. J. Quantum Chem.* **106**, 2173 (2006).
180. J. Carrasco *et al.*, *Phys. Stat. Sol. C* **2**, 153 (2005).
181. Y. F. Zhukovskii, E. A. Kotomin, S. Piskunov and D. E. Ellis, *Solid State Commun.* **149**, 1359 (2009).
182. L. Grigorjeva, D. Millers, E. A. Kotomin and E. S. Polzik, *Solid State Commun.* **104**, 327 (1997).
183. E. Possenriede, B. Hellerman and O. F. Schirmer, *Solid State Commun.* **65**, 31 (1988).
184. E. A. Kotomin *et al.*, *Phys. Rev. B* **60**, 1 (1999).
185. R. I. Eglitis, E. A. Kotomin and G. Borstel, *Phys. Stat. Sol. B* **208**, 15 (1998).
186. A. L. Shluger and A. M. Stoneham, *J. Phys.: Condens. Matter* **5**, 3049 (1993).
187. J. T. Devreese *et al.*, *Phys. Rev. B* **63**, 184304 (2001).
188. G. Borstel, R. I. Eglitis, E. A. Kotomin and E. Heifets, *J. Cryst. Growth* **237–239**, 687 (2002).
189. B. Faust, H. Müller and O. F. Schirmer, *Ferroelectrics* **153**, 297 (1994).
190. M. Gao, S. Kapphan, R. Pankrath and J. Zhao, *Phys. Stat. Sol. B* **217**, 999 (2000).
191. R. I. Eglitis, E. A. Kotomin and G. Borstel, *J. Phys.: Condens. Matter* **14**, 3735 (2002).
192. R. I. Eglitis *et al.*, *J. Phys.: Condens. Matter* **14**, L647 (2002).
193. R. I. Eglitis *et al.*, *Comput. Mater. Sci.* **27**, 81 (2003).
194. E. A. Kotomin, R. I. Eglitis and G. Borstel, *J. Phys.: Condens. Matter* **12**, L557 (2000).
195. H. J. Reyher, Private Communication (2001).
196. S. Köhne *et al.*, *J. Supercond.* **12**, 193 (1999).
197. S. Lenjer, O. F. Schirmer, H. Hesse and T. Kool, *Phys. Rev. B* **66**, 165106 (2002).
198. V. S. Vikhnin, R. I. Eglitis, P. A. Markovin and G. Borstel, *Phys. Stat. Sol. B* **212**, 53 (1999).
199. R. I. Eglitis, E. A. Kotomin and G. Borstel, *J. Phys.: Condens. Matter* **12**, L431 (2000).

Ab initio calculations of ABO_3 perovskite surfaces and defects

200. R. I. Eglitis *et al.*, *Mater. Sci. Semicond. Process.* **5**, 153 (2003).
201. R. I. Eglitis, E. A. Kotomin, G. Borstel and S. Dorfman, *J. Phys.: Condens. Matter* **10**, 6271 (1998).
202. J. H. Crawford, *Nucl. Instrum. Methods Phys. Res. B* **1**, 159 (1984).
203. K. L. Yip and W. B. Fowler, *Phys. Rev. B* **11**, 2327 (1975).